Geomicrobiology Journal, 19:253–287, 2002

0149-0451/02 $12.00 + .00

Theoretical and Experimental Considerations Related to Reaction-Based Modeling: A Case Study Using Iron(III) Oxide Bioreduction

WILLIAM D. BURGOS
RICHARD A. ROYER
YILIN FANG

Department of Civil and Environmental Engineering
The Pennsylvania State University
University Park, Pennsylvania, USA

GOUR-TSYH YEH

Department of Civil and Environmental Engineering
University of Central Florida
Orlando, Florida, USA

ANGELA S. FISHER
BYONG-HUN JEON
BRIAN A. DEMPSEY

Department of Civil and Environmental Engineering
The Pennsylvania State University
University Park, Pennsylvania, USA

The kinetics of reductive dissolution of hematite (α-Fe_2O_3) by the dissimilatory iron-reducing bacterium Shewanella putrefaciens *strain CN32 under nongrowth conditions with H_2 as the electron donor was measured and then modeled using a reaction-based biogeochemical model. Minimum data needs and a reaction matrix decomposition procedure are presented from a reaction-based modeling perspective and used to design subsequent experiments. Detailed step-by-step modeling methodology is presented. Independent experiments were performed to determine if Fe^{2+} sorption to* S. putrefaciens *CN32 or hematite could be described as either kinetic or equilibrium reactions (i.e., slow or fast, respectively, relative to the time-scale of the bioreduction experiments). Fe^{2+} sorption to* S. putrefaciens *CN32 was an equilibrium reaction and a linear adsorption isotherm was used to determine the associated equilibrium constant. Fe^{2+} sorption*

Received 21 December 2000; accepted 5 November 2001.

This research was supported by the Natural and Accelerated Bioremediation Research Program (NABIR), Office of Biological and Environmental Research (OBER), U.S. Department of Energy (DOE) Grant No. DE-FG02-98ER62691 with The Pennsylvania State University. Dr. G. T. Yeh was also supported by the Biogeochemical Program, National Science Foundation (NSF) under Grant EAR-0196048 with University of Central Florida. Preprocessor in BIOGEOCHEM available upon request from G. T. Yeh (gyeh@mail.ucf.edu).

Address correspondence to William D. Burgos, Department of Civil Engineering, The Pennsylvania State University, 212 Sackett Building, University Park, PA 16802-1408, USA. E-mail: bburgos@psu.edu

to hematite was a kinetic reaction and an elementary rate formulation was independently determined from abiotic experiments. The ratio of the forward rate divided by the backward rate [$\log(k^f/k^b)$] for the sorption of Fe^{2+} to hematite was 6.33 ± 0.14 ($n = 2$) and the corresponding $\log(k^f)$ was 6.66 ± 0.28 ($n = 2$, $M^{-1}\ h^{-1}$). Three different kinetic reaction rate formulations were used to model hematite bioreduction, an elementary rate law for the overall reaction, an empirical rate law physically based on hematite "free" surface sites, and an empirical rate law physically based on hematite free surface sites and bacterial inhibition caused by Fe(II) biosorption. All rate formulations modeled the measured results reasonably well (R^2 values ranged from 0.83 to 0.99). For the elementary rate formulation, $\log(k^f/k^b)$ was 24.37 ± 0.15 ($n = 4$) and the corresponding forward rate [$\log(k^f)$] was 26.46 ± 0.27 ($n = 4$, $M^{-4}\ h^{-1}$). These results demonstrate that independently determined reaction-based rate formulations were applicable in another experimental system, as theoretically expected. Therefore, the simulation and prediction of complex biogeochemical systems may eventually be able to be performed using reaction-based models.

Keywords iron reduction, kinetic modeling, *Shewanella*, ferrous sorption, biosorption

The biogeochemistry of microbial Fe(III) reduction and of associated contaminant interactions is very complex. Because multiple simultaneous reactions often occur under Fe(III)-reducing conditions it is difficult to adequately characterize all operative reactions. For example, bioreduction of ferric oxide will produce biogenic Fe(II) and secondary reactions of Fe(II) may include sorption/surface complexation to mineral surfaces, aqueous complexation (if complexants present) (Urrutia et al. 1999; Zachara et al. 2000), precipitation of ferrous minerals (Fredrickson et al. 1998), biosorption to bacterial cells (Urrutia et al. 1998; Liu et al. 2001a), and re-oxidation. Stimulation of dissimilatory iron-reducing bacteria (DIRB) may be a feasible strategy for the in situ bioremediation of both organic and inorganic contaminants via both direct and indirect means. Aromatic contaminants (e.g., benzene and toluene, Lovley et al. 1994) can be directly used as electron donors by certain DIRB. Nitroaromatics (Heijman et al. 1995; Klausen et al. 1995) and chlorinated aliphatics (Curtis and Reinhard 1994; Kim and Picardal 1999) can be indirectly reduced by (biogenic) surface-sorbed Fe(II). A variety of metals [e.g., Cr(VI)] and radionuclides [e.g., U(VI), Tc(VII)] can be directly reduced by DIRB or indirectly reduced by biogenic Fe(II) (Lovley 1993; Fredrickson et al. 2000; Wildung et al. 2000).

To properly evaluate and design engineered systems that stimulate biological Fe(III) reduction for contaminant remediation, appropriate biogeochemical kinetic models are needed. To be most useful and applicable to varied environmental settings, chemical reaction-based versus ad hoc models are specifically needed. Distinctions between chemical reaction-based versus ad hoc *models* (Yeh et al. 2001) or mechanistic versus empirical *rate formulations* (Steefel and van Cappellen 1998) have been noted and discussed extensively (e.g., Yeh and Tripathi 1989). Reaction-based models simulate and formulate the production-consumption rate of every chemical species due to every chemical reaction (both equilibrium and kinetic) while ad hoc models do not consider all reactions influencing a species (Yeh et al. 2001).

In an empirical approach, an empirical function is used to fit experimental data to determine reaction parameters. In a mechanistic-based approach, a rate formulation is derived from proposed reaction pathways. A mechanism consists of a sequence of elementary reactions that describes how the final products are formed from the initial reactants and determines the overall reaction. Either type of model could use empirical or mechanistic rate formulations to simulate kinetic reactions (although ad hoc models often use empirical formulations). The advantage of using a reaction-based model (versus ad hoc model), even

when an empirical rate formulation is used, is that these formulations are theoretically descriptive of the chemical reaction and, therefore, applicable to a range of environmental conditions (versus only those of the experiment). The disadvantage of using a reaction-based model is that the proposition of the reaction network and the determination of the mechanism are difficult. Although ad hoc models using empirical rate formulations may guarantee a "fit" with the data, they may limit the ability of the model to describe other systems because individual processes are not independently determined. On the other hand, mechanistic models, admittedly ambitious, aim at representing the fundamental processes occurring in the system, which will be extremely difficult in complex natural systems (Steefel and van Cappellen 1998).

We have reviewed relevant literature to compile Fe(II) production rates that were explicitly reported by the authors or that we calculated from their data. In Table 1, the term "rate" is liberally used. In many cases rates were extracted from experiments that were not designed to yield such information because of bacterial growth conditions or infrequent time-course sampling. Rates listed do not include more than two significant digits because data used for their calculation were estimated from associated figures. Table 1 summarizes results obtained with solid-phase ferric oxides (crystalline and noncrystalline) and in some cases with and without the soluble electron-shuttling compound anthraquinone-2,6-disulfonate (AQDS). These summaries reveal that microbial pure culture, microbial conditions (e.g., growth versus nongrowth), electron donor, medium components (e.g., P), and buffer (e.g., HCO_3^- versus organic-based) can all exert an effect on bioreduction kinetics. The presence of carbonate and phosphate are particularly important because the precipitation of siderite and vivianite, respectively, will reduce the activity of Fe^{2+} and/or may passivate the surfaces of ferric oxides. Noncrystalline hydrous ferric oxide (HFO) is typically reduced more quickly than crystalline oxides (e.g., Lovley and Phillips 1988; Zachara et al. 1998), and AQDS can have a significant effect on enhancing the rate of Fe(III) reduction (e.g., Fredrickson et al. 1998; Lovley et al. 1998).

Several studies have shown that Fe(II) production rates may be first order with respect to oxide surface area (therefore, surface sites) regardless of oxide crystallinity (Arnold et al. 1986; Roden and Zachara 1996; Roden and Urrutia 1999). However, normalization of rates to surface area does not account for all variance and Zachara et al. (1998) have proposed that molecular scale characteristics (e.g., crystalline disorder, microheterogeneities) may also exert an effect on bioreduction.

The primary objective of this paper is to discuss both theoretical aspects of reaction-based kinetic models and practical aspects of experimental measurements related to the biological reduction of solid-phase Fe(III) oxides. A secondary objective is to describe reaction-based modeling procedures for the reaction-based software BIOGEOCHEM (Fang et al. 2002) in a detailed step-by-step manner for those less familiar with biogeochemical modeling. Minimum data needs for reaction-based modeling, introduced from a theoretical perspective, are often a significant experimental burden. As the number of chemical species and reactions operative in an experimental system increase, so do the minimum data needs. Therefore, "model" systems with characterized materials and controlled conditions were used to reduce the minimum data needs and make reaction-based modeling a tractable activity. The biological reduction of crystalline hematite (α-Fe_2O_3) by the dissimilatory-iron reducing bacterium *Shewanella putrefaciens* strain CN32 under nongrowth conditions with H_2 as the electron donor was studied. This experimental system yielded the fewest chemical species and smallest reaction network for modeling purposes. Separate experiments were designed to evaluate whether important chemical reactions, notably Fe^{2+} sorption to hematite and *S. putrefaciens* CN32, were kinetic or equilibrium

TABLE 1 Bioreduction kinetics of solid phase Fe(III) oxides reported in or calculated from data contained in peer-reviewed literature

Organism	Fe(III) source	Electron donor	Buffer/Medium	Rate (μM Fe(II) h^{-1})[a]	Comments on source data	Reference
Geobacter metallireducens $C_i = 10^6$ cell mL^{-1}[b]	100 mM HFO[c]	20 mM Acetate	30 mM HCO_3^-, pH 7.0, 5.0 mM P, 0 or 50 μM AQDS, defined medium	670—with AQDS; 280—w/o AQDS	Bacterial growth conditions; T = 30°C; Rates estimated from zero-order regression through first 5-d data shown on Figure 1.	Nevin and Lovley 2000
Geobacter metallireducens $C_i = 10^6$ cell mL^{-1}	100 mM HFO; 100 mM Goethite; 100 mM Hematite	20 mM Lactate	30 mM HCO_3^-, pH 7.0, 5.0 mM P, 0 or 100 μM AQDS; defined medium	570—HFO with AQDS; 160—HFO w/o AQDS; 520—Goethite with AQDS; 30—Goethite w/o AQDS; 70—Hematite with AQDS; 7.0—Hematite w/o AQDS;	Bacterial growth conditions; T = 30°C; HFO rates estimated from zero-order regressions through first 4-d data shown on Figure 3 (significant cell increases). Goethite and hematite rates estimated from zero-order regressions through first 3-h data shown on Figure 5.	Lovley et al. 1998
Geobacter metallireducens $C_i = 10^6$ cell mL^{-1}	Synthetic HFO; Natural HFO; Akaganeite; Goethite; Hematite (all 200 mM)	10 mM Acetate	30 mM HCO_3^-, pH 7.0, 5.0 mM P, defined medium	490—synthetic HFO; 590—natural HFO; 9.4—Akaganeite; 7.3—Goethite; 6.3—Hematite;	Bacterial growth conditions; T = 30°C; Rate estimated from single 4-d data point listed in Table 3.	Lovley and Phillips 1988
Geobacter sulfurreducens PCA $C_i = 10^6$ cell mL^{-1}	100 mM HFO	30 mM Lactate	30 mM HCO_3^-, pH 7.0, 5.0 mM P, defined medium	1,110 (Figure 2A); 440 (Table 1)	Bacterial growth conditions; T = 35°C; Rate estimated from zero-order regression through first 15-h data shown on Figure 2A. Also, rate estimated from single 5-d data point listed in Table 1.	Caccavo et al. 1992

Shewanella putrefaciens CN32 $C_i = 2$ to 4 (10^8) cell mL^{-1}	45 mM HFO	27 mM Lactate	30 mM PIPES, pH 7.1, 0 or 3.9 mM P, 0 or 100 μM AQDS; defined medium	1700 with AQDS and P; 1400 with AQDS and w/o P; 340 w/o AQDS and with P; 270 w/o AQDS and w/o P	Bacterial growth conditions; T = 30°C; Rates estimated from zero-order regressions through first 16-h data shown on Figure 5b.	Fredrickson et al. 1998
Shewanella putrefaciens CN32 $C_i =$ $(2.4)10^8$ cell mL^{-1}	50 mM HFO; 50 mM Goethite; 50 mM Hematite	27 mM Lactate	30 mM HCO_3^-, pH 6.9, 3.9 mM P, 0 or 100 μM AQDS; defined medium	300—HFO with AQDS; 26—HFO w/o AQDS; 73—Goethite with AQDS; 5.4—Goethite w/o AQDS; 20—Hematite with AQDS; 2.0—Hematite w/o AQDS;	Bacterial growth conditions; T = 30°C; Rates estimated from single 4-d data point shown on Figures 1a and 17.	Zachara et al. 1998
Shewanella putrefaciens CN32 $C_i = 10^8$ cell mL^{-1}	25 mM Hematite	H_2 overpressure	50 mM PIPES, pH 6.8, 0 mM HCO_3^-, 0.03 mM P, 0 or 50 μ M AQDS	10 w/o AQDS; 110 with AQDS;	Nongrowth conditions; T = 20°C; Rates estimated from zero-order regressions through first 4-h data w/ AQDS and 16-h data w/o AQDS.	Current study; Burgos et al. 2002
Shewanella putrefaciens 200 $C_i = 1.8(10^6)$ cell mL^{-1}	Lepidocrocite; Goethite (both 45 mM)	20 mM Lactate	10 mM HEPES, pH 7.0–7.3, 0.5 mM HCO_3^-, 0.044 mM P, defined medium	160—Lepidocrocite; 90—Goethite	Bacterial growth conditions; Room temperature; Rates reported in text.	Cooper et al. 2000
Shewanella putrefaciens 200 $C_i = 2(10^9)$ cell mL^{-1}	HFO (all 1.9 mM); Goethite; Lepidocrocite; Hematite	16 mM Lactate	pH = 7.0 w/pH-stat, 0 mM HCO_3^-, 2.9 mM P, defined medium	1,000—HFO; 20—Geothite; 18—Lepidocrocite; 12—Hematite	Chemostat operation; T = 31°C; Rates taken from rates shown on Figure 6 for "no chelator" condition.	Arnold et al. 1988

(Continued on next page)

TABLE 1 Bioreduction kinetics of solid phase Fe(III) oxides reported in or calculated from data contained in peer-reviewed literature *(Continued)*

Organism	Fe(III) source	Electron donor	Buffer/Medium	Rate (μM Fe(II) h^{-1})[a]	Comments on source data	Reference
Shewanella putrefaciens 200 $C_i = 2(10^9)$ cell mL^{-1}	1.86 mM $FeCl_3$ freshly precipitated	16 mM Lactate	pH-stat controlled, 0 mM HCO_3^-, 2.9 mM P, defined medium	1,100 (pH 6.5–7.0); 820 (pH 7.5)	Chemostat operation; T = 31°C; Rates taken from rates shown on Figure 4a at [%Fe(III) remaining] = 100% (i.e., fastest initial rates).	Arnold et al. 1986
Shewanella algae BrY $C_i = 10^8$ cell mL^{-1}	40 mM HFO; HSA[c]-Goethite; MSA-Goethite (both Gt 50 mM)	H_2 overpressure + 30 mM malate as C-source	10 mM PIPES, pH 6.9, 0 mM HCO_3^-, 4.4 mM P, defined medium	640—HFO; 200—HSA-Gt; 40—MSA-Gt	Bacterial growth conditions; T = 31°C; Rates taken from rates shown on Figures 5C, 5D, and 5E at t = 0 d (i.e., fastest initial rates).	Urrutia et al. 1998
Shewanella algae BrY $C_i = 2(10^8)$ cell mL^{-1}	HFO; HSA-Goethite; MSA-Goethite; LSA-Goethite; Hematite	30 mM Lactate	10 mM PIPES, pH 7.0, 4.4 mM P, defined medium	600—HFO; 1,400—HSA-Gt; 180—MSA-Gt; 140—LSA-Gt; 7.2—Hematite	Bacterial growth conditions; T = 30°C; Rates taken from rates shown on Figure 1 at [Initial Fe(III)] = 200 mM for HFO, or [Initial Fe(III)] = 250 mM for all other oxides.	Roden and Zachara 1996
Desulfuromonas acetoxidans $C_i = 2(10^7)$ cell mL^{-1}	100 mM HFO	5 mM Acetate	30 mM HCO_3^-, pH 7.0, 5.0 mM P, defined medium	125	Bacterial growth conditions; T = 30°C; Rate estimated from zero-order regression through first 10-d data shown on Figure 3A.	Roden and Lovley 1993

[a]Rate of biogenic Fe(II) production calculated from authors' source data.
[b]Cell suspension concentration inoculated at t = 0.
[c]HSA—high surface area, MSA—medium surface area, LSA—low surface area, HFO—hydrous ferric oxide.

reactions. For kinetic reactions, further experiments were designed to independently parameterize these processes. For equilibrium reactions, further experiments were designed to measure the associated equilibrium constants. Kinetic rate formulations and equilibrium constants obtained from these independent experiments were used along with several rate formulations to model hematite bioreduction kinetics. Theoretically, reaction-based rate formulations are descriptive of the chemical reaction and, therefore, applicable to conditions other than those used for their determination. Thus, using independently obtained kinetic and equilibrium parameters allowed a means to challenge the model and our theoretical approach.

Kinetic Modeling

In numerical modeling of reaction-based biogeochemical processes, the evolution of M chemical species can be described by the principle of chemical kinetics as follows (Stumm and Morgan 1996):

$$\frac{dC_i}{dt} = \sum_{k=1}^{N} (\nu_{ik} - \mu_{ik}) R_k, \quad i \in M, \tag{1}$$

where C_i is the concentration of the i-th chemical species, N is the number of biogeochemical reactions, ν_{ik} is the reaction stoichiometry of the i-th species in the k-th reaction associated with the products, μ_{ik} is the reaction stoichiometry of the i-th species in the k-th reaction associated with the reactants, R_k is the rate of the k-th reaction. In BIOGEOCHEM, species concentrations are all in mol L^{-1}, including solid-phase and sorbed species. Equation 1 is a mass balance for any species i in a reactive system that states that the rate of change of mass of any species is due to all reactions that produce or consume this species.

An analytical solution of equation 1 is generally not possible, although numerical integration can be attempted. Numerical integration of equation 1 will encounter two major difficulties. First, the rates of N reactions can, in general, range over several orders of magnitude. If at least one of the reaction rates is orders of magnitude faster than the time-scale of interest, the time-step size must be extremely small relative to the time-scale of interest, which makes integration impractical. Second, for most practical problems the number of independent reactions is less than the number of species. This implies that there are one or more chemical components whose masses must be conserved during the reactions. To facilitate numerical integration, equation 1 is manipulated to decouple fast reactions from slow reactions and to explicitly enforce mass conservation of chemical components. The manipulation is achieved via either the Gauss-Jordan elimination (Chilikapati 1995; Steefel and MacQuarrie 1996; Chilikapati et al. 1998) or the QR decomposition (Chen 1994) of the reaction matrix.

A mathematical decomposition of equation 1 is used to determine the number of linearly independent reactions (N_I) and to select mass-conserved chemical components (N_C). The investigator identifies the number of linearly independent equilibrium reactions (N_E) based on certain assumptions. The decomposition of equation 1 then reduces a set of M simultaneous ordinary differential equations governing the production-consumption of M species into three subsets of equations: N_E nonlinear algebraic equations representing mass action laws and/or user-specified algebraic equations for the equilibrium reactions; $(N_I - N_E)$ simultaneous ordinary differential equations representing the rate of change of the kinetic-variables; and N_C linear algebraic equations representing mass conservation

of the chemical components (where $M = N_I + N_C$). These equation subsets are defined as:

Mass action equations for equilibrium reactions

$$\frac{dE_i}{dt} = D_{kk}R_k + \sum_{j \in N_{KD(k)}} D_{ij}R_j; \quad i = 1, 2, \ldots, N_E; \quad k \in N_E : \Rightarrow \; R_k = \infty \tag{2}$$

Kinetic-variables equations

$$\frac{dE_i}{dt} = D_{kk}R_k + \sum_{j \in N_{KD(k)}} D_{ij}R_j; \quad i = N_E + 1,\ N_E + 2, \ldots, N_I - N_E; \quad k \in N_{KI} \quad \text{where} \quad E_i = \sum_{j=1}^{M} b_{ij}C_j \quad \text{and} \tag{3}$$

Mass conservation equations for N_C chemical components

$$\frac{dT_i}{dt} = 0; \quad i = 1,\ 2, \ldots, N_C \quad \text{where} \quad T_i = \sum_{j=1}^{M} b_{ij}C_j \tag{4}$$

where E_i is the i-th kinetic-variable; D_{kk} is the diagonal term of the decomposed reaction matrix; $N_{KD(k)}$ is the subset of linearly dependent kinetic reactions, which depends on the k-th reaction; N_{KI} is the number of linearly independent kinetic reactions; b_{ij} is the i-th row and j-th column of the matrix resulting from the Gauss-Jordan decomposition of the unit matrix of size $M \times M$; and T_i is the i-th component. A kinetic-variable is defined as a linear combination of species concentrations. The slope of a kinetic-variable-versus-time measures the rate of a kinetic reaction when no other kinetic reactions depend on this reaction. Alternatively, a "lumped" kinetic-variable can be defined when several parallel reactions contribute to the evolution of the same species. Thus, a kinetic-variable is distinct from a time-variant chemical species concentration in that the evolution of a chemical species depends on all kinetic reactions this species participates in, while the evolution of a kinetic-variable depends on only one kinetic reaction (or several parallel reactions for a lumped kinetic-variable). The significance of a kinetic-variable is that it can be used to parameterize the reaction rate of the associated kinetic reaction (or lumped parallel reactions) independent of other kinetic reactions.

The decomposition of equation 1 to equations 2–4 is not unique, that is, a large number of equation subsets are possible. The decomposition is not unique because the selection of chemical components for a system is not unique (Yeh et al. 2001). This nonuniqueness allows an adaptation of governing equations for robust numerical solutions. However, the selection of the chemical components can be one of the most daunting aspects of these kinds of problems. For example, the decomposition preprocessor of BIOGEOCHEM (Fang et al. 2002) may generate a set of components that are difficult to grasp intuitively (e.g., a negative total hydrogen concentration) yet are mathematically correct.

A reaction-based geochemical code was developed to solve equations 2–4 (Salvage and Yeh 1998; Fang et al. 2002) and simulate the production-consumption of all species concentration-versus-time. Having obtained the concentrations of all species, the concentrations of each of the $(N_I - N_E)$ kinetic-variables-versus-time can be plotted. The slope

of each curve would represent the rate of a kinetic reaction if all kinetic reactions were linearly independent. Knowing the rates of kinetic reactions, reaction rate formulations can be evaluated in an iterative fashion one reaction at a time. The most straight forward approach to formulating a rate equation is to assume an elementary rate law for the overall reaction:

$$R_k = \left(K_k^f \prod_{i=1}^{M} (A_i)^{\mu_{ik}} - K_k^b \prod_{i=1}^{M} (A_i)^{\nu_{ik}} \right)$$

$$= \left(k_k^f \prod_{i=1}^{M} (C_i)^{\mu_{ik}} - k_k^b \prod_{i=1}^{M} (C_i)^{\nu_{ik}} \right), \quad k \in (N_I - N_E) \tag{5}$$

$$\text{with} \quad k_k^f = K_k^f \prod_{i=1}^{M} (\gamma_j)^{\mu_{ik}} \quad \text{and} \quad k_k^b = K_k^b \prod_{i=1}^{M} (\gamma_i)^{\nu_{ik}}$$

where K_k^f is the forward rate constant and K_k^b is the backward rate constant of the k-th reaction, k_k^f is the modified forward rate constant and k_k^b is the modified backward rate constant of the k-th kinetic reaction, A_i is the activity of the i-th species, and γ_i is the activity coefficient of the i-th species. Note that k_k^f and k_k^b are numerically equal to K_k^f and K_k^b, respectively, when the activity coefficients of all species are assumed to equal 1. In BIOGEOCHEM, chemical activity (distinct from concentration) is dependent on the type of species. The default value for all activity coefficients is 1. For aqueous ionic species the Davies equation is used to calculate activity coefficients based on either a user-specified or program-calculated ionic strength. For adsorbed species the activity coefficient is set equal to 1, thus activity is equal to concentration. For ion-exchanged species, the activity is proportional to the ion-exchanged mole fractions. For solid phase species the activity is set equal to 1. It should be noted that activity is used in mass action equations and for rate formulation purposes, and that concentration is used in all mass conservation equations.

If this first iteration is inadequate, a rate formulation is proposed based on our understanding of the experimental system. Either physically based empirical or mechanistic-based approaches may be taken. In an empirical approach, a rate formulation is proposed and reaction parameters including rate constants are determined from the analysis of kinetic-variable concentration-versus-time profiles. In a mechanistic-based approach, a rate formulation is derived from proposed reaction pathways.

Experimental Methods

Microorganism and Culture Conditions

The DIRB *Shewanella putrefaciens* CN 32 was provided from the Subsurface Microbial Culture Collection courtesy of Dr. David Balkwill (Florida State University). All cells used were grown aerobically on tryptic soy broth without dextrose (Difco) at 20°C. The cells for the inoculation of each experiment were harvested by centrifugation (3510 × g, 10 min, 15°C) from a 16-h-old culture (late log-decreasing growth phase). The cells were washed three times in 50 mM PIPES (pH = 6.8)–30 μM phosphate (added as K_2HPO_4 and KH_2PO_4) buffer (hereafter referred to as PIPES-phosphate buffer), with the last washing being made with deoxygenated solution. The final cell pellet was resuspended in 7–20 mL of deoxygenated PIPES-phosphate buffer in a Coy anaerobic chamber under a N_2:H_2 (97.5:2.5) atmosphere and the cell density determined by absorbance at 420 nm.

Iron(III) oxide. Hematite (α-Fe_2O_3) from J. T. Baker had a specific surface area of 9.04 m^2g^{-1} measured by 5-point BET-N_2 adsorption. Mössbauer spectroscopy and X-ray diffraction did not reveal any impurities. Hematite suspensions were prepared in anaerobic PIPES-phosphate buffer at least 24 h before use to allow for complete surface hydration.

Analytical techniques. In the various experiments the following parameters were routinely measured or recorded: dissolved Fe(II), acid-extractable Fe(II), total Fe(II), total Fe, pH, $H_2(g)$, and temperature. Dissolved Fe(II) was measured with filtered (0.1 μm aluminum oxide) sample aliquots added to 5 mL of ferrozine reagent (1 g L^{-1} ferrozine in 50 mM HEPES, pH = 8.0) in the anaerobic chamber. After 10 min the samples were removed, absorbance at 562 nm was determined with a Shimadzu UV/Vis-1601 spectrophotometer, results were corrected for dilution and converted to Fe(II) by comparison with standards. Acid-extractable Fe(II) was determined by adding a 1-mL sample aliquot to 4 mL of 0.625 N HCl to achieve a final normality of 0.5 N. The solution was then removed from the anaerobic chamber and allowed to mix for 2 h. For the sorption experiments, the 0.5 N HCl extraction period was 24 h. The samples were then filtered (0.1 μm) and the filtrate was analyzed as per the dissolved Fe(II) analysis. Total Fe(II) was measured in the abiotic sorption experiments by acidifying the sample to achieve a final normality of 3.0 N HCl, filtering (0.1 μm) the sample, reacting the sample with ammonium fluoride to eliminate the interference of soluble Fe(III) (Tamura et al. 1974), and then using the 1,10-phenanthroline colorimetric method (APHA 1995) to measure total Fe(II). For analytical consistency, all Fe(II) measurements in the abiotic experiments used the 1,10-phenanthroline method. Total Fe was determined by adding a 1-mL sample aliquot to 4 mL of 0.625 N HCl along with 0.5 g sodium dithionite per 20–50 mg hematite. The solution was allowed to mix for 24 h, filtered, and then analyzed as per the dissolved Fe(II) analysis. For samples with *S. putrefaciens* CN32 and hematite, several additions of dithionite over several days were required to obtain a final constant value. Solution pH was determined by combination electrode on sample filtrate in the anaerobic chamber. $H_2(g)$ was recorded from the Coy gas meter (Grass Lake, MI) in the anaerobic chamber. Temperature was recorded from a digital thermometer in the anaerobic chamber. All experiments were performed in a 20°C constant temperature room.

Fe^{2+} sorption to hematite. Significant measures were taken to eliminate any trace contamination of O_2 during Fe^{2+} sorption experiments. Milli-Q water was first purged with O_2-free N_2 for 24 h, and then brought into the anaerobic chamber where it was magnetically stirred for another 24 h. All dry reagents were equilibrated in the anaerobic chamber for at least 24 h before use. Dry reagents were weighed on an analytical balance in the anaerobic chamber to prepare all solutions and suspensions. The anaerobic chamber interlock was never opened during the Fe^{2+} sorption experiments (i.e., all analytical reagents and instruments were either inside the chamber, or preserved samples were all removed at the end of the experiment). A 2.00 g L^{-1} suspension of hematite was prepared in PIPES-phosphate buffer and spiked with 10.0 mg L^{-1} of Fe^{2+} (added as acidified $FeCl_2$) at t = 0 h and magnetically mixed in the anaerobic chamber. At times of t = 1, 5, 10, 15, 30, and 60 min; 2, 4, and 24 h; and 5 d, triplicate samples were collected and analyzed for dissolved Fe(II), acid-extractable Fe(II), total Fe(II), total Fe, and pH. This experiment was replicated twice.

Fe^{2+} sorption to S. putrefaciens CN 32. The kinetics of Fe^{2+} sorption to *S. putrefaciens* CN32 was measured with 10^8 cells mL^{-1} suspension in PIPES-phosphate buffer spiked with 4.3 mg L^{-1} of Fe^{2+} (added as acidified $FeCl_2$) at t = 0 min and magnetically mixed in the anaerobic chamber. At times of t = 1, 5, 10, 20, 30 min, and 24 h, triplicate samples were collected and analyzed for dissolved Fe(II), acid-extractable Fe(II), and pH. Once it was

established that equilibrium was rapid and invariant after 10 min, a series of experiments were conducted to generate an adsorption isotherm. A single master reactor suspension of 10^8 cells mL^{-1} was prepared in PIPES-phosphate buffer and incrementally spiked with Fe^{2+} concentrations of 5, 7.5, 10, and 12.5 mg L^{-1}. After each Fe(II) spike, triplicate samples were removed, transferred into 10-mL amber serum bottles, sealed with Teflon-faced butyl rubber stoppers and aluminum crimp seals, and mixed. After 24 h, samples were collected and analyzed for dissolved Fe(II), acid-extractable Fe(II), and pH. *S. putrefaciens* CN32-sorbed Fe(II) (i.e., DIRB-Fe^{2+}) was calculated as the difference between acid-extractable and dissolved Fe(II).

Bioreduction of hematite. Test systems for kinetic bioreduction experiments consisted of 180 mL of suspension in 250-mL serum bottles. Bottles were periodically opened to the anaerobic chamber atmosphere (for sample collection) to provide a constant concentration of dissolved H_2(aq) and minimize evaporation during all experiments. H_2(g) concentrations were recorded within the anaerobic chamber and always remained constant (2.5%) over the complete time-course of each experiment. A 2.00 g L^{-1} hematite suspension in PIPES-phosphate buffer was inoculated to achieve a final cell density of 10^8 cells mL^{-1}. Time-course samples were collected to measure dissolved Fe(II), acid-extractable Fe(II), total Fe, and pH. Triplicate samples were collected at each sampling event and the kinetic experiment was replicated four times. Uninoculated (abiotic) controls were incubated in quintuplicate and sampled once after t = 5 d.

Modeling Methods

General description. Eight steps are described for reaction-based modeling. First, once a reaction network is proposed to describe the system, the N reactions should be numbered and arranged in any order. Typically, the most important chemical reaction is listed first (i.e., R1) followed by all others. Second, the M species should be arranged in any order. Typically, the species are ordered as they appear in the ordered reactions (e.g., reactant #1 in R1 is assigned M1). Third, the rank of the reaction matrix (N_I) is presumed and the identity of the mass conserved species (N_C) among the M species are guessed.

Fourth, a formal decomposition of the reaction matrix is performed using the preprocessor in BIOGEOCHEM (Fang et al. 2002). If the guessed number of components or component species are not correct, the preprocessor will automatically make corrections based on a detailed decomposition procedure. This automatic correction procedure involves the removal of a guessed-component species during a column reduction step. If a pivot can be found from rows other than those corresponding to the guessed-components, then the guess is likely correct. Otherwise, a row corresponding to the guessed-component must be chosen as the pivot and this species will not be a component anymore.

These third and fourth steps may have to be performed several times. The most important outcome of the matrix decomposition is to select chemical components that yield (1) the most important kinetic-variable equation (i.e., central process under investigation) and (2) at least one mass conservation equation in terms of species (or operational quantities) that can all be experimentally measured.

Fifth, the concentrations of all species are computed based on N_{KI} measured quantities, N_C mass conservation equations, and N_E mass action equations with best estimates or independent measurements of equilibrium constants for all equilibrium reactions. The computation of all species concentrations at this step is accomplished with any solver of simultaneous linear and nonlinear algebraic equations (e.g., Mathematica). Sixth, the reaction rates for all kinetic reactions as a function of time are obtained from the slopes of the kinetic-variable concentration-versus-time curves. A reaction rate is measured by the slope

of a kinetic-variable-versus-time curve, *not* by the slope of a species concentration-versus-time curve. Although in simple systems a kinetic-variable may consist of a single species, the distinction between a kinetic-variable and a species cannot be overemphasized.

Seventh, reaction rate formulations are proposed and tested, and associated rate parameters are determined. By matching the rates from experimental measurements with those from the rate formulations, the rate parameters are solved for over several time intervals. The number of data points in each time interval must equal the number of parameters characterizing the reaction rates. For example, a rate formulation with two parameters will need to be solved over a time interval that includes two estimates of the rate (i.e., two equations, two unknowns). This seventh step is used to narrow the range of values of the reaction parameters. Eighth, simulations of the reaction network are conducted (i.e., solve the systems of mass action equations, kinetic-variable equations, and component mass conservation equations using the proposed reaction rate formulations and parameters) and compared with experimental data. The simulations are performed using the reaction-based numerical code BIOGEOCHEM (Fang et al. 2002) to yield the production-consumption of all species concentration-versus-time. The seventh and eighth steps constitute an iterative procedure to minimize the error between the measured and simulated species concentration-versus-time, and must be repeated until satisfactory results are obtained.

Bioreduction example. For the described bioreduction experiments a reaction network of 9 reactions ($N = 9$) and 12 species ($M = 12$) was hypothesized (Table 2). H_2O was not included as a species because its activity was assumed to equal 1. First, the bioreduction of hematite was our primary objective and was assigned reaction number R1. The remaining eight reactions were not arranged in a specific order (but similar reactions were grouped together). Experimental evidence suggested that R2–R4 and R8–R9 were equilibrium reactions, thus $N_E = 5$. Second, the species were arranged in order of their appearance in the reactions (e.g., Fe_2O_3 assigned species number M1, H_2(aq) assigned species number M2, etc...). Third, an initial value of the rank of the reaction matrix was presumed to be $N_I = 7$. Thus, the initial required number of chemical components was $N_C = M - N_I = 5$ and the number of linearly independent kinetic-variables was $N_{KI} = N_I - N_E = 2$. We then guessed/assigned Fe_2O_3, H_2(aq), H^+, PIPES, and DIRB as the five component species.

Fourth, a formal matrix decomposition was performed with our preprocessor to yield five mass conservation equations, equations 8.1–8.5 in Table 2. This decomposition confirmed the initial rank of the reaction matrix $N_I = 7$. For this first decomposition we obtained mass conservation equation 8.1 in which all terms on the right hand side of the equation were measured (total Fe using 0.5 N HCl + dithionite procedure). When this measured quantity was plotted versus time, it remained constant and validated partial system consistency (this subset of the data not shown). System consistency is defined as when all mass conservation equations are satisfied *and* confirmed with experimental data (Yeh et al. 2001). Partial system consistency means that at least one of the N_C mass conservation equations can be confirmed with direct experimental evidence. The minimum number of chemical species concentration-versus-time that must be measured to evaluate the kinetic suite of reactions using a reaction-based model is $(N_I - N_E)$ (Yeh et al. 2001). For the bioreduction experiment, two kinetic quantities were measured, Fe^{2+}(aq) and 0.5 N HCl Fe(II), as required by $N_{KI} = N_I - N_E = 2$. The 0.5 N HCl Fe(II) concentration was assumed to equal the kinetic-variable ($[Fe^{2+}] + [=FeOFe^{(II)+}] + [DIRB\text{-}Fe^{2+}]$). We note three additional quantities were measured, namely total Fe, pH, and H_2(g). However, these three quantities were used for other purposes and were not required as members of N_{KI}. Total Fe was used to assess partial system consistency (equation 8.1), H_2(g) was used to indirectly measure

TABLE 2 Reaction network, matrix decomposition, and reaction-based rate formulation for the biological reduction of hematite (α-Fe_2O_3). All Fe species are in (+III) valence unless designated $Fe^{(II)+}$ or Fe^{2+}

Bacterial reduction of hematite		Reaction parameters
$Fe_2O_3 + H_2(aq) + 4H^+ \leftrightarrows 2Fe^{2+} + 3H_2O$	(R1)	Eq. 9.1
Surface "hydration" of hematite		
$Fe_2O_3 + 3H_2O \leftrightarrows 2[(OH)_2 = FeOH]$	(R2)	$\log K^e_{TSS} = -1.91$
Surface acidity		
$=FeOH_2^+ \rightleftarrows =FeOH + H^+$	(R3)	$\log K^e_3 = -7.31$
$=FeOH \rightleftarrows =FeO^- + H^+$	(R4)	$\log K^e_4 = -8.93$
Sorption of Fe^{2+} to hematite		
$=FeOH_2^+ + Fe^{2+} \leftrightarrows =FeOFe^{(II)+} + 2H^+$	(R5)	
$=FeOH + Fe^{2+} \leftrightarrows =FeOFe^{(II)+} + H^+$	(R6)	R567 $\rightarrow$ Eq. 12.1a
$=FeO^- + Fe^{2+} \leftrightarrows =FeOFe^{(II)+}$	(R7)	
Biosorption of Fe^{2+}		
$DIRB + Fe^{2+} \leftrightarrows DIRB\text{-}Fe^{2+}$	(R8)	$\log K^e_8 = +1.43$
PIPES buffering		
$HPIPES \leftrightarrows PIPES^- + H^+$	(R9)	$\log K^e_9 = -6.80$

N_E Mass action equations

$$\frac{1}{2}\frac{d([=FeOH_2^+] + [=FeOH] + [=FeO^-] + [=FeOFe^{(II)+}])}{dt} = R_2: \tag{6.1a}$$

$$(R_2 = \infty \Rightarrow)^a \quad [=FeOH] = (K^e_2)^{1/2}[Fe_2O_3]^{1/2}$$

$$\frac{1}{2}\frac{d([=FeOH_2^+] + [=FeOH] + [=FeO^-] + [=FeOFe^{(II)+}])}{dt} = R_2: \; R_2 = \infty \Rightarrow$$

$$[=FeOH]_T = K^e_{TSS}[Fe_2O_3] = [=FeOH_2^+] + [=FeOH] + [=FeO^-] + [=FeOFe^{(II)+}] \tag{6.1b}^b$$

$$\textit{where} \quad K^e_{TSS} = \frac{S_A N_s}{N_A} M_{Fe_2O_3}$$

$$\frac{d([=FeOH_2^+] + [=FeOFe^{(II)+}])}{dt} = -R_3 + R_6 + R_7: \tag{6.2}$$

$$R_3 = \infty \Rightarrow [=FeOH_2^+] = \frac{1}{K^e_3}[=FeOH][H^+]$$

$$\frac{d[=FeO^-]}{dt} = R_4 - R_7: \tag{6.3}$$

$$R_4 = \infty \Rightarrow [=FeO^-] = K^e_4 \frac{[=FeOH]}{[H^+]}$$

(Continued on next page)

TABLE 2 Reaction network, matrix decomposition, and reaction-based rate formulation for the biological reduction of hematite (α-Fe_2O_3). All Fe species are in (+III) valence unless designated $Fe^{(II)+}$ or Fe^{2+} *(Continued)*

$$\frac{d[DIRB - Fe^{2+}]}{dt} = R_8: \tag{6.4}$$

$$R_8 = \infty \Rightarrow [Fe^{2+}] = \frac{1}{K_8^e}\frac{[DIRB - Fe^{2+}]}{[DIRB]}$$

$$\frac{d[HPIPES]}{dt} = -R_9 : \; R_9 = \infty \Rightarrow [HPIPES] = \frac{1}{K_9^e}[PIPES^-][H^+] \tag{6.5}$$

($N_I - N_E$) Kinetic-variable equations

$$\frac{1}{2}\frac{d([Fe^{2+}] + [{=}FeOFe^{(II)+}] + [DIRB - Fe^{2+}])}{dt} = R_1 \tag{7.1}$$

$$\frac{d[{=}FeOFe^{(II)+}]}{dt} = R_5 + R_6 + R_7 = R_{567} \tag{7.2}$$

N_C Mass conservation equations

$$TOT_{Fe_2O_3} = [Fe_2O_3] + \frac{1}{2}[{=}FeOH_2^+] + \frac{1}{2}[{=}FeOH] + \frac{1}{2}[{=}FeO^-] + [{=}FeOFe^{(II)+}] + \frac{1}{2}[Fe^{2+}] + \frac{1}{2}[DIRB - Fe^{2+}] \tag{8.1}$$

$$TOT_{H_2} = [H_2(aq)] + \frac{1}{2}[Fe^{2+}] + \frac{1}{2}[{=}FeOFe^{(II)+}] + \frac{1}{2}[DIRB - Fe^{2+}] \tag{8.2}$$

$$TOT_{H^+} = [H^+] + [{=}FeOH_2^+] - [{=}FeO^-] + [{=}FeOFe^{(II)+}] + [HPIPES] + 2[Fe^{2+}] + 2[DIRB - Fe^{2+}] \tag{8.3}$$

$$TOT_{DIRB} = [DIRB] + [DIRB - Fe^{2+}] \tag{8.4}$$

$$TOT_{PIPES} = [PIPES^-] + [HPIPES] \tag{8.5}$$

Kinetic reaction rate formulations

$$R_1 = k_1^f[H_2(aq)][H^+]^4 - k_1^b[Fe^{2+}]^2 \tag{9.1a}$$

$$R_1 = k_{fss}([{=}FeOH_2^+] + [{=}FeOH] + [{=}FeO^-]) \tag{9.1b}$$

$$R_1 = k_{pass}([{=}FeOH_2^+] + [{=}FeOH] + [{=}FeO^-]) - k_{inhib}[DIRB - Fe^{2+}] \tag{9.1c}$$

$$R_5 + R_6 + R_7 = R_{567} = k_{567}^f[{=}FeO^-][Fe^{2+}] - k_{567}^b[{=}FeOFe^{(II)+}] \tag{12.1a}$$

[a] ($R_2 = \infty \Rightarrow$) is shorthand notation designating that when reaction rate R_2 is "infinitely" large, the mass action equation will yield the following ($\Rightarrow$) expression.

[b] Refer to equation 16 in text for definition of terms.

H_2(aq) which was used to determine TOT_{H2} (equation 8.2), and pH was used to determine TOT_{H^+} (equation 8.3).

Fifth, Mathematica (Wolfram Research, Champaign, IL) was used to compute all 12 species concentration-versus-time using 12 equations [equations 6.1b, 6.2–6.5, 8.1–8.5, and two equations for the measured kinetic quantities Fe^{2+}(aq) and 0.5 N HCl Fe(II)]. Sixth, the concentration of the kinetic-variable ($[Fe^{2+}] + [=FeOFe^{(II)+}] + [DIRB\text{-}Fe^{2+}]$)-versus-time was plotted and the slopes were determined at all times. We did not plot the concentration of the second kinetic-variable $[=FeOFe^{(II)+}]$-versus-time because the lumped reaction rates R_5, R_6, and R_7 (referred to as R_{567}) had been independently formulated and determined (described in next example).

Seventh, reaction rate formulations were proposed for R_1. An elementary rate law (equation 9.1a, Table 2) was proposed first. Because this rate formulation had two parameters, two points from the measured rates were used to set up two equations to solve for the parameters k_1^f and k_1^b. This procedure was repeated for three sets where each set included two rates at two time points. Eighth, simulations were conducted by solving 12 simultaneous equations (equations 6.1b, 6.2–6.5, 8.1–8.5, 12.1a, and 9.1a, b, or c) for the evolution of TOT_{H^+}, TOT_{H2}, and 10 species ($[H^+]$ and $[H_2(aq)]$) were measured and constant, thus two components plus 10 species were simulated, not 12 species) using BIOGEOCHEM.

Instead of using the iterative optimization procedure of steps seven and eight, a graphical optimization procedure can first be used to evaluate the feasibility of a proposed rate formulation, and provide initial estimates of rate parameters for steps seven and eight. Because all species concentration-versus-time (in step five) and the reaction rate-versus-time (in step six) have been calculated, these data can be manipulated according to the proposed rate equation to estimate the rate parameters. For example, to obtain an initial estimate of the rate parameters for the elementary rate formulation (equation 9.1a), this equation can be manipulated to yield:

$$\frac{R_1}{[Fe^{2+}]^2} = k_1^f \frac{[H_2(aq)][H^+]^4}{[Fe^{2+}]^2} - k_1^b \tag{13}$$

Equation 13 can be plotted as $R_1/[Fe^{2+}]^2$ versus $\{([H_2(aq)][H^+]^4)/[Fe^{2+}]^2\}$ to determine k_1^f (from the slope) and $-k_1^b$ (from the y-intercept) (Figure 1A). We may assume that this is a reasonable rate formulation for R_1 because the R^2 of this regression is high (0.999) and this goodness-of-fit criterion was maintained with all four replicate experiments.

Other rate formulations were used to determine if better matches between simulations and measurements could be obtained. A physically based empirical formulation of R_1 was proposed to be first-order with respect to free hematite surface sites (equation 9.1b). To determine an initial estimate of the rate parameter for equation 9.1b, we plot R_1 versus $([=FeOH_2^+] + [=FeOH] + [=FeO^-])$ and k_{fss} will be equal to the slope (Figure 1B). These data reveal that a first-order relationship with respect to free surface sites was maintained only for the first ca. 14 h, and then beyond this point the relationship failed. A poor correlation to free surface sites was observed in two of our four experiments suggesting that this rate formulation may be less feasible.

A second physically based empirical formulation of R_1 (equation 9.1c) was proposed to be first-order with respect to free hematite surface sites (to capture effect of hematite surface "passivation") and first-order with respect to the biosorbed Fe(II) concentration (to capture effect of DIRB "inhibition" by Fe(II) sorption to cell wall). To determine an initial

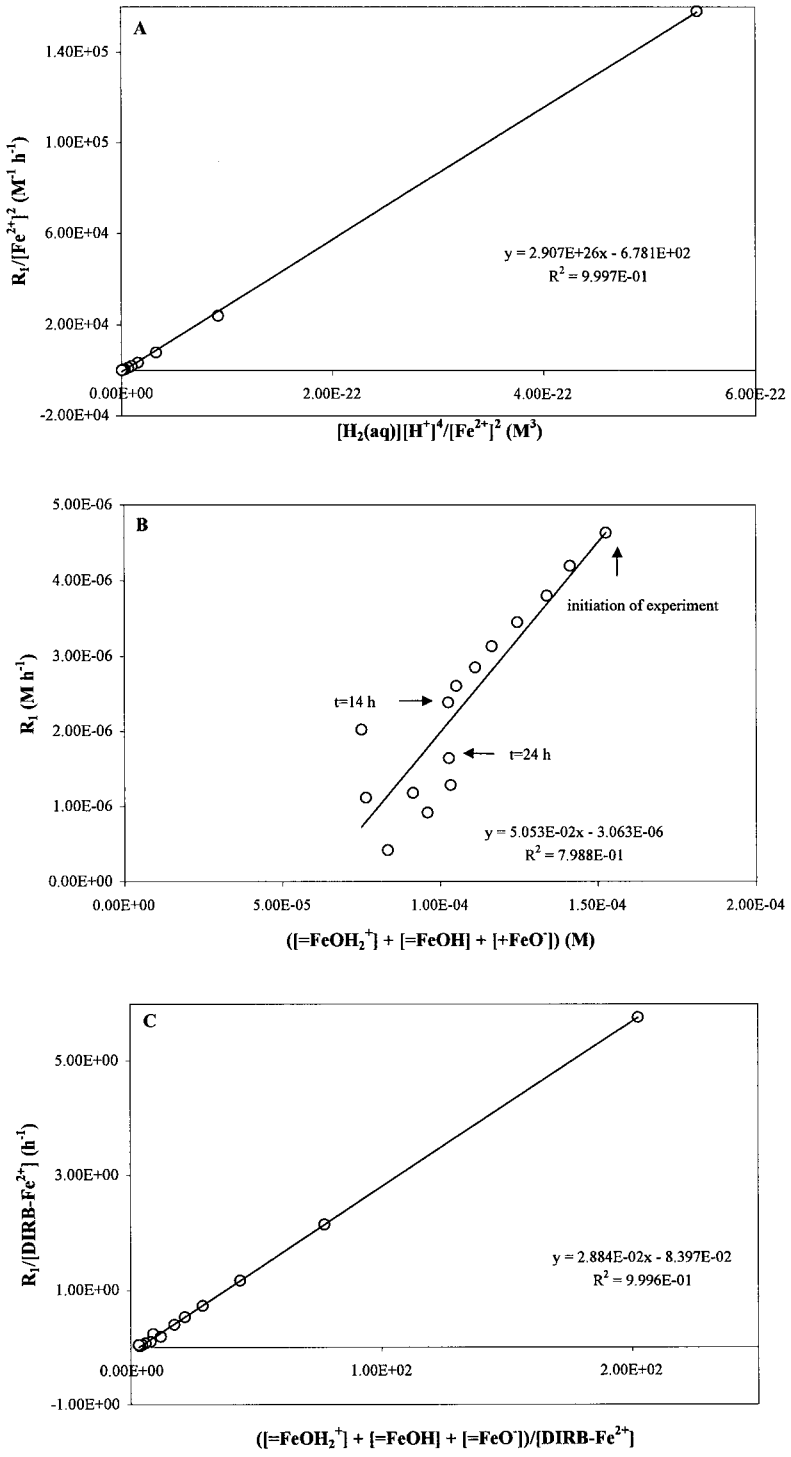

FIGURE 1 Graphical manipulation of calculated reaction rate (R1) and species concentration-versus time to test proposed rate formulations and obtain initial estimates of associated rate parameters. (A) Elementary rate formulation (equation 9.1a). (B) Empirical rate formulation based on "free" surface sites (equation 9.1b). (C) Empirical rate formulation based on surface passivation and DIRB inhibition (equation 9.1c). Results shown are for the biological reduction of hematite-Replicate # 1.

estimate of the rate parameters for equation 9.1c, this equation can be manipulated to yield:

$$\frac{R_1}{[\text{DIRB} - \text{Fe}^{2+}]} = k_{pass}\frac{([=\text{FeOH}_2^+] + [=\text{FeOH}] + [\text{FeO}^-])}{[\text{DIRB} - \text{Fe}^{2+}]} - k_{inhib} \qquad (14)$$

Equation 14 can be plotted as $R_1/[\text{DIRB-Fe}^{2+}]$ versus $\{([=\text{FeOH}_2^+] + [=\text{FeOH}] + [=\text{FeO}^-])/[\text{DIRB-Fe}^{2+}]\}$ to determine k_{pass} (from the slope) and $-k_{inhib}$ (from the y-intercept) (Figure 1C). We may assume that this is a reasonable rate formulation for R_1 because the R^2 of this regression is high (0.999) and this goodness-of-fit criterion was maintained with all four replicate experiments. The objective of the graphical estimation procedure is to optimize parameters based on the rate of the reaction. The objective of the iterative procedure in steps seven and eight is to minimize the error between the measured and simulated species concentration-versus-time, and this procedure should be used for final parameter estimates.

Abiotic sorption example. For the described abiotic sorption experiments, a reaction network of seven reactions (N = 7) and nine species (M = 9) was hypothesized (Table 3). A similar eight-step procedure could be presented, however, only certain steps will be discussed for brevity. In the fourth step, a matrix decomposition yielded mass conservation equation 11.1 (Table 3) in which all terms on the right hand side of the equation were measured [0.5 N HCl Fe(II)] so that partial system consistency was assessed for this system. A plot of equation 11.1 [Figure 1, $TOT_{Fe(II)}$ assumed to equal 0.5 N HCl Fe(II)] should remain constant as a function of time if our reaction network is correct and complete; however, the recovery of Fe(II) decreased throughout the experiment. An acceptable recovery of Fe(II) was assumed to be 95% of the added mass and this was maintained for the first 120 min. The loss of total measurable Fe(II) could be due to a surface transformation of hematite-sorbed Fe(II) to magnetite (Coughlin and Stone 1995; Jeon et al. 2001). Inclusion of this process and the sorption of Fe^{2+} to newly formed magnetite in the current reaction network would significantly increase minimum data needs. Therefore, only the data collected within the first 120 min, during which equation 11.1 was assumed valid with the hypothesized reaction network, were used to model the lumped kinetic reactions R5–R7 (referred to as R_{567}).

The sorption of Fe^{2+} to hematite occurred in a distinct two-stage manner (Figures 2 and 3). Within 1 min, Fe^{2+} decreased from 10 to 8 mg L^{-1} but after 120 min Fe^{2+} had further decreased to 7.5 mg L^{-1}. No single rate formulation for R_{567} was able to model the results from t = 0 to t = 120 min. Because the focus of this work is on hematite bioreduction where Fe^{2+} was slowly produced and never instantaneously added, we decided that a rate formulation for the second, slower phase was more relevant for modeling bioreduction. Therefore, the 1-min data were used as initial conditions for modeling the second-stage sorption kinetics ($1 \leq t \leq 120$ min).

In the seventh step, reaction rate formulations for the lumped contribution of R_{567} were proposed. An elementary rate law for the overall reaction R_{567} (equation 12.1a) was proposed first. The forward and backward rate constants in equation 12.1a were lumped parameters given by:

$$k_{567}^f = \frac{k_5^f[H^+]^2}{K_3^e K_4^e} + \frac{k_6^f[H^+]}{K_4^e} + k_7^f; \quad k_{567}^b = k_5^b[H^+]^2 + k_6^b[H^+] + k_7^b, \qquad (15)$$

where k_{567}^f and k_{567}^b are the lumped forward and backward rate constants for R_{567}, k_5^f and k_5^b are the forward and backward rate constants for R5, k_6^f and k_6^b are the forward and backward rate constants for R6, k_7^f and k_7^b are the forward and backward rate constants for

TABLE 3 Reaction network, matrix decomposition, and reaction-based rate formulation for the abiotic sorption of Fe^{2+} to hematite (α-Fe_2O_3)

Surface "hydration" of Hematite		Reaction parameters
$Fe_2O_3 + 3H_2O \leftrightarrows 2[(OH)_2 = FeOH]$	(R2)	$\log K^e_{TSS} = -1.91$
Surface acidity		
$=FeOH_2^+ \rightleftarrows =FeOH + H^+$	(R3)	$\log K^e_3 = -7.31$
$=FeOH \rightleftarrows =FeO^- + H^+$	(R4)	$\log K^e_4 = -8.93$
Sorption of Fe^{2+} to hematite		
$=FeOH_2^+ + Fe^{2+} \leftrightarrows =FeOFe^{(II)+} + 2H^+$	(R5)	
$=FeOH + Fe^{2+} \leftrightarrows =FeOFe^{(II)+} + H^+$	(R6)	R5-R7 → Eq. 12
$=FeO^- + Fe^{2+} \leftrightarrows =FeOFe^{(II)+}$	(R7)	
PIPES buffering		
$HPIPES \leftrightarrows PIPES^- + H^+$	(R9)	$\log K^e_9 = -6.80$

N_E Mass action equations

$$\frac{d[=FeOH_2^+]}{dt} = -R_3 - R_5: \qquad (10.1)$$

$$(R_3 = \infty \Rightarrow)^a\ [=FeOH_2^+] = \frac{1}{K^e_3}[=FeOH][H^+]$$

$$\frac{d[=FeO^-]}{dt} = R_4 - R_7: \qquad (10.2)$$

$$R_4 = \infty \Rightarrow [=FeO^-] = K^e_4 \frac{[=FeOH]}{[H^+]}$$

$$\frac{1}{2}\frac{d([=FeOH_2^+] + [=FeOH] + [=FeO^-] + [=FeOFe^{(II)+}])}{dt} = R_2 :\ R_2 = \infty \Rightarrow$$

$$[=FeOH]_T = K^e_{TSS}[Fe_2O_3] = [=FeOH_2^+] + [=FeOH] + [=FeO^-] + [=FeOFe^{(II)+}] \qquad (6.1b)^b$$

$$\textit{where}\quad K^e_{TSS} = \frac{S_A N_s}{N_A} M_{Fe_2O_3}$$

$$\frac{d[HPIPES]}{dt} = -R_9 :\ R_9 = \infty \Rightarrow [HPIPES] = \frac{1}{K^e_9}[PIPES^-][H^+] \qquad (6.5)$$

$(N_I - N_E)$ Kinetic-variable equations

$$\frac{d[=FeOFe^{(II)+}]}{dt} = R_5 + R_6 + R_7 = R_{567} \qquad (7.2)$$

N_C Mass conservation equations

$$TOT_{Fe(II)} = [=FeOFe^{(II)+}] + [Fe^{2+}] \qquad (11.1)$$

(Continued on next page)

TABLE 3 Reaction network, matrix decomposition, and reaction-based rate formulation for the abiotic sorption of Fe^{2+} to hematite (α-Fe_2O_3) *(Continued)*

$$TOT_{Fe_2O_3} = [Fe_2O_3] + \frac{1}{2}[=FeOH_2^+] + \frac{1}{2}[=FeOH] + \frac{1}{2}[=FeO^-] + \frac{1}{2}[=FeOFe^{(II)+}] \quad (11.2)$$

$$TOT_{H^+} = [H^+] + [=FeOH_2^+] - [=FeO^-] - [=FeOFe^{(II)+}] + [HPIPES] \quad (11.3)$$

$$TOT_{PIPES} = [PIPES^-] + [HPIPES] \quad (8.5)$$

Kinetic reaction rate formulations

$$R_5 + R_6 + R_7 = R_{567} = k^f_{567}[=FeO^-][Fe^{2+}] - k^b_{567}[=FeOFe^{(II)+}] \quad (12.1a)$$

$$R_5 + R_6 + R_7 = R_{567} = k^F_{567}([=FeOH_2{}^+] + [=FeOH] + [=FeO^-])$$

$$- k^B_{567}[=FeOFe^{(II)+}] \quad (12.1b)$$

All Fe species are in (+III) valence unless designated $Fe^{(II)+}$ or Fe^{2+}.

[a] $(R_3 = \infty \Rightarrow)$ is shorthand notation designating that when reaction rate R_3 is "infinitely" large, the mass action equation will yield the following ($\Rightarrow$) expression.

[b] Refer to equation 16 in text for definition of terms.

R7, and K^e_3 and K^e_4 are the equilibrium constants for R3 and R4. It is clear from equation 15 that the lumped forward and backward rate constants depend on pH. However, because pH remained constant in the abiotic experiments, k^f_{567} and k^b_{567} were considered constants. To segregate these three reactions, separate experiments would have to performed at pH values where one reaction was predominantly operative at a time. A physically based empirical

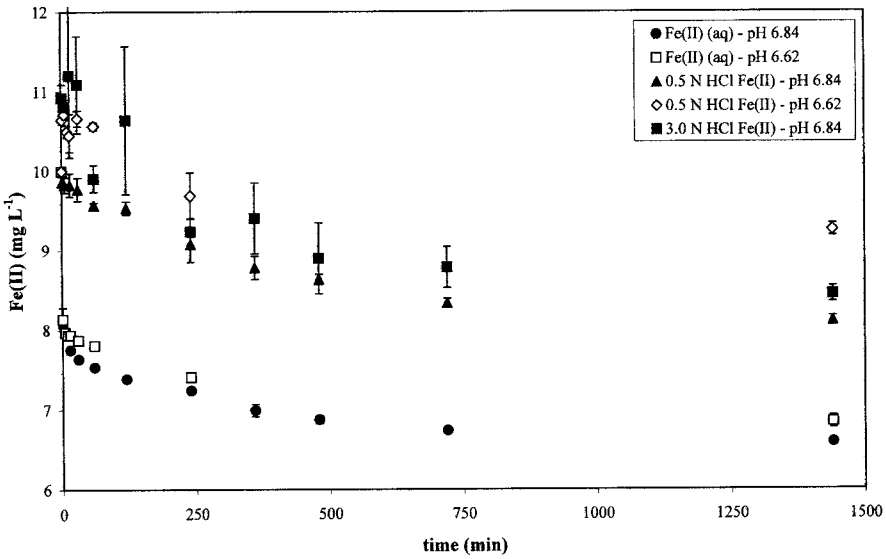

FIGURE 2 Reaction kinetics for the abiotic sorption of Fe^{2+} to hematite over first 24 h. HCl acid extractions revealed incomplete recovery of Fe(II). Error bars represent standard deviation of triplicate measurements.

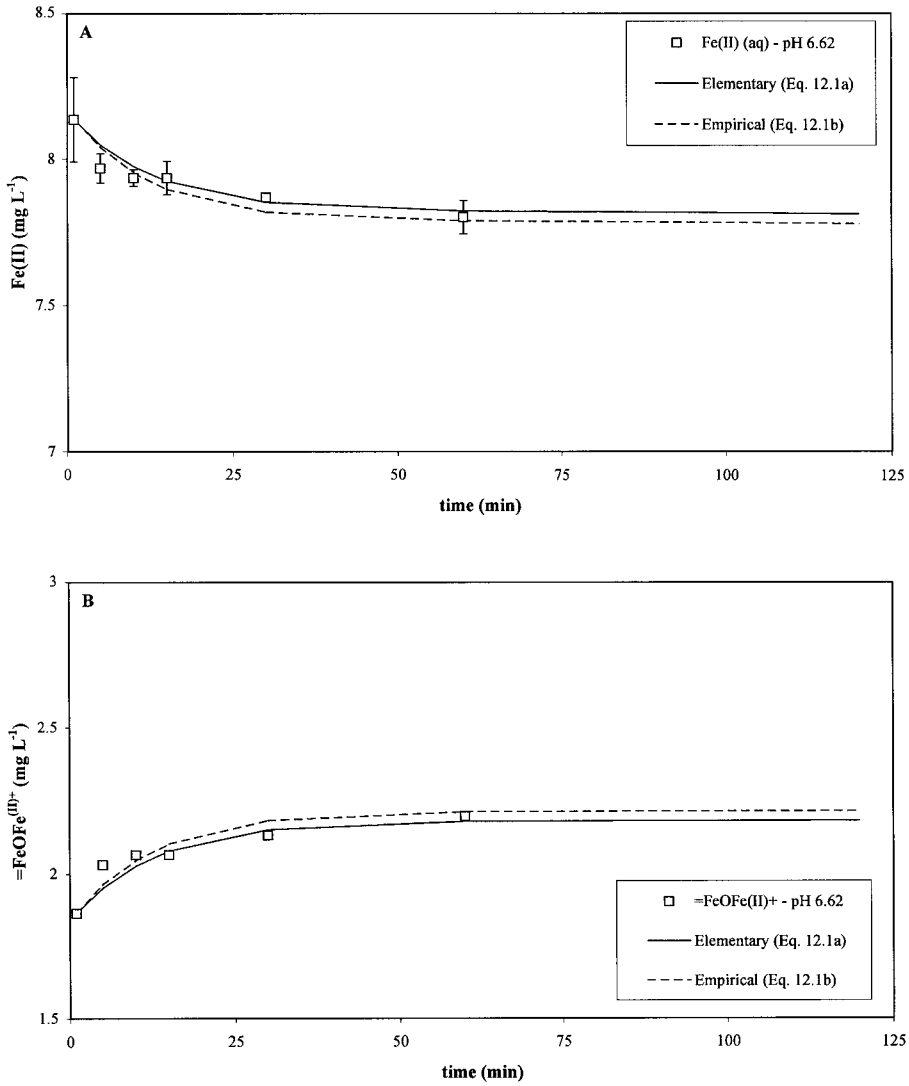

FIGURE 3 Sorption kinetics of Fe^{2+} to hematite at pH 6.62. (A) Fe(II) (aq) loss from solution over first 120 min. (B) Corresponding production of $=FeOFe^{(II)+}$. Both an elementary rate formulation (equation 12.1a) and an empirical rate formulation (equation 12.1b) were used to model the experimental results. Rate parameters are given in Table 4. Error bars represent standard deviation of triplicate measurements.

rate formulation (equation 12.1b) was assumed to be first-order with respect to free hematite surface sites and first-order with respect to $=FeOFe^{(II)+}$.

Results and Discussion

Approach and Assumptions

In this paper we apply a reaction-based model to the bioreduction of hematite. The experiments were designed to yield a small, tractable number of chemical species and reactions.

The reaction network proposed in Table 2 is based on a number of significant assumptions. Nongrowth conditions were maintained in these experiments so that the biomass concentration (designated as the species DIRB in Table 2) was assumed to remain constant. In separate experiments performed under identical conditions, bacterial viability remained between 93 to 99% after 5 d of incubation as measured by direct counts using the LIVE/DEAD *Bac*light viability stain (Molecular Probes, Eugene, OR) thus validating this assumption.

Phosphate was assumed to not affect the experimental results and reactions for vivianite precipitation and phosphate sorption to hematite were excluded from the reaction network. Quintuplicate cultures with and without 30 μM phosphate were tested in 1- and 5-d experiments and there was no detectable statistical difference between the two treatments. These results do not validate that these phosphate reactions did not occur but simply demonstrate that phosphate played no significant role in these experiments.

The formation of magnetite cannot be controlled by exclusion of certain medium components; however, experiments identical to the ones described here revealed no statistical difference between biogenic Fe(II) measured with 0.5 N or 3.0 N HCl extractions (biogenic magnetite is presumably soluble in 3 N HCl). Therefore, reactions for magnetite formation were excluded from the reaction network.

Hydrogen was chosen as the electron donor to eliminate carbonate from the system and all associated reactions such as siderite precipitation and carbonate sorption to hematite. A constant partial pressure of $H_2(g)$ was maintained in the anaerobic chamber above the reactors (therefore, constant $[H_2(aq)]$). Experiments were designed in this manner because measuring the consumption of $H_2(g)$ in the headspace of a sealed serum bottle as a function of time was not possible due to gas volume requirements and analytical precision. One result of this approach is that the mass conservation equation 8.2 (Table 2) appears suspect since $H_2(aq)$ is always replenished in the system. When the experimental system is open with respect to a particular component (e.g., TOT_{H2}), then the external supply of the component to the system is assumed to maintain a constant concentration of the component species (e.g., $[H_2(aq)]$). Under such circumstances the mass conservation equation is no longer a mass conservation equation for the species, but is decoupled from the system and used to account for the total amount of the component mass replenished to the system. Therefore, equation 8.2 should not be viewed as a mass conservation equation for hydrogen, rather it should be viewed as a mass accounting equation for the total amount of hydrogen replenished to the system. Importantly, this is the correct mathematical formulation for this experimental system.

The other result of using an "open" system with a constant partial pressure of $H_2(g)$ is that trace amounts of oxygen in the anaerobic chamber may interfere with the experiment (e.g., as alternative electron acceptor or as Fe(II) oxidant). However, on two separate occasions reactor contents were removed from the "open" master reactors at $t = 0$, transferred to serum bottles, sealed with Teflon-faced butyl rubber stoppers and aluminum crimp tops, incubated alongside the master reactor, and sacrificed for chemical analyses. There was no detectable statistical difference between the "open" and "closed" vessels based on the measured dissolved $Fe^{2+}(aq)$ and 0.5 N HCl Fe(II) concentrations on either occasion. These results suggest that the "open" master reactors were not significantly affected by trace amounts of oxygen in the anaerobic chamber (possibly due to the facultative nature of *S. putrefaciens* CN32).

For the kinetic reactions R1 and R_{567} an elementary rate law was used to describe the overall reactions. An elementary reaction describes a reaction that actually occurs as written at the molecular level (Lasaga 1998), and the collision theory can be used to describe reaction kinetics (Atkins 1986). The complexity and stoichiometry of R1 clearly show that this is not an elementary reaction. The biological reduction of hematite would occur through

a series of elementary reactions mediated by different bacterial enzymes. We have presented detailed mechanistic rate formulations for R1 in this manner (Yeh et al. 2001). These rate formulations were not used in this current work because minimum data needs were not met for the correspondingly more complicated reaction networks. However, an elementary rate formulation for the overall reaction may be a good approximation when the reaction is not far from equilibrium as it would reduce to the mass action equation at equilibrium.

Equilibrium Reactions

Preliminary experiments or literature references were used to determine all equilibrium reaction constants. We have determined or assumed that the hematite surface hydration (R2), hematite surface acidity (R3, R4), Fe^{2+} biosorption (R8), and PIPES buffering (R9) reactions are all "fast" (i.e., at equilibrium) relative to our time-scale of interest (Knapp 1989). For reaction-based modeling, a balanced chemical reaction is required for all processes. Therefore, certain assumptions were needed to describe the hematite surface hydration reaction (R2) used to distinguish between the bulk and surface species. Reaction R2 is applicable to certain crystalline oxide surfaces (e.g., 001 face of hematite) where surface atoms are coordinated to three surface hydroxyls; however, we applied this stoichiometry to the whole hematite surface area. Mass action equation 6.1a (Tables 2 and 3) would be obtained based upon the stoichiometry of R2. This equation was not used in these simulations because the stoichiometry of R2 is not likely maintained for all hematite surface atoms, and two kinetic rate formulations (equations 9.1b, 9.1c; Table 1) for hematite bioreduction (R1) were based on "free" hematite surface sites [i.e., $\sum([=FeOH_2^+] + [=FeOH] + [=FeO^-])$].

Instead, the "user-specified" mass action equation 6.1b was used to distinguish between the bulk and surface species. Surface site species concentration are related to the mineral suspension concentration by (Stumm and Morgan 1996):

$$\begin{aligned}[=FeOH]_T &= [=FeOH] + [=FeOH_2^+] + [FeO^-] + [=FeOFe^{(II)+}] \\ &= K^e_{TSS}[Fe_2O_3] \qquad (16)\end{aligned}$$

$$\text{with} \quad K^e_{TSS} = \frac{S_A N_s}{N_A} MW_{Fe_2O_3}$$

where $[=FeOH]_T$ is the total hematite surface site concentration (mol sites L^{-1}), K^e_{TSS} is the lumped equilibrium constant for the total surface sites, S_A is the hematite unit surface area ($m^2\ g^{-1}$), N_S is the surface site density (mol sites m^{-2}), N_A is Avagadro's number (mol sites mol^{-1}), $MW_{Fe_2O_3}$ is the molecular weight of hematite (g mol^{-1}), and $[Fe_2O_3]$ is the hematite suspension concentration (mol L^{-1}). Because this is a user-specified equation, we have chosen to use the concentration of $[Fe_2O_3]$ instead of its activity (assumed to equal 1 for solid species). Estimates for hematite surface site density ranged from 1.2 sites nm^{-2} based on proton-titration data to 5.1 sites nm^{-2} based on Fe^{2+} adsorption isotherm data (Jeon et al. 2001). These values fall within the wide range of site density values (e.g., 1 to 10 sites nm^{-2}) that have been used to describe adsorption to ferric oxides. For the current modeling study we have assumed a site density of 5.1 sites nm^{-2} specifically based on Fe^{2+} adsorption isotherm data. Using the estimated value of 5.1 sites nm^{-2} and the measured surface area of 9.04 $m^2\ g^{-1}$, $\log K^e_{TSS}$ for equation 6.1b was then calculated to equal -1.91.

The initial distribution of $[=FeOH]_T$ between $[=FeOH_2^+]$, $[=FeOH]$, and $[=FeO^-]$ surface species can be calculated based upon pH and the hematite surface acidity constants K^e_3 and K^e_4. Surface acidity constants for hematite were assumed to equal -7.31 and -8.93 for $\log K^e_3$ and $\log K^e_4$, respectively (Dzombak and Morel 1990). The equilibrium constant

for PIPES buffering ($\log K_8^e = -6.80$) was based on product information (Sigma-Aldrich, St. Louis, MO).

Fe^{2+} Sorption to Hematite

The sorption of 10.0 mg L^{-1} Fe^{2+} to 2.00 g L^{-1} hematite in PIPES-phosphate buffer at pH 6.62 ± 0.01 and pH 6.84 ± 0.01 was shown to be a kinetic reaction (Figure 2). The reaction network for this experiment, its decomposition, and kinetic rate formulations are summarized in Table 3. The reaction network includes three parallel kinetic reactions (R5, R6, R7) that yield the same product (=FeOFe$^{(II)+}$). Parallel kinetic reactions cannot be uniquely segregated when they contribute to the production of the same species (Yeh et al. 2001). Thus, individual reaction-based rate formulations for these kinetic reactions could not be determined from this experiment alone even if the minimum number of species concentration-versus-time were measured. Instead, only a rate formulation that effectively lumped these three parallel reactions together (R_{567}) could be formulated and tested. Since our primary goal was to evaluate R1, a formulation for the lumped contribution of R_{567} (equation 12.1a or 12.1b, Table 3) was acceptable.

The sorption of Fe^{2+} to ferric oxide is a complicated process. The loss of recoverable Fe(II) is one indication that hematite-sorbed Fe(II) undergoes a topotactic conversion into another mineral phase that is insoluble in 0.5 N HCl. Thus, the kinetics of Fe^{2+} sorption are also complicated, reflecting both rapid cation exchange/surface complexation reactions and slow surface binding/surface transformation reactions. However, when we modeled only the slow second-stage ($1 \leq t \leq 120$ min) of Fe^{2+} sorption to hematite, acceptable fits were obtained with either an elementary (equation 12.1a) or empirical rate formulation (equation 12.1b) (Figures 3 and 4, Table 4). Model estimates of the rate constants for both rate formulations obtained with both experiments and goodness-of-fit criterion are summarized in Table 4. For an elementary reaction rate formulation the forward rate divided by the backward rate equals the equilibrium constant for the overall reaction. For the two abiotic sorption experiments this ratio was $\log(k^f_{567}/k^b_{567}) = 6.33 \pm 0.14$ ($n = 2$) (Table 4), and this estimate of the equilibrium constant would correspond to a ΔG° of -36.1 kJ mol^{-1}. By comparison, the ΔG° for the adsorption of zinc and cadmium to hydrous ferric oxide has been reported to equal -20.5 and -19.4 kJ mol^{-1}, respectively (Trivedi and Axe 2000). The averaged elementary rate constants used in the bioreduction simulations were determined from the average of the forward rate constants [$\log(k^f_{567}) = 6.66 \pm 0.28$ M^{-1} hr^{-1}], and the backward rate constant was then calculated using the average $\log(k^f_{567}/k^b_{567})$ value to obtain $\log(k^b_{567}) = 0.33 \pm 0.14$ (M^{-1} hr^{-1}).

Figures 3 and 4 show that either rate formulation could fit the data. However, when the independently determined elementary rate formulation (equation 12.1a) was used in the simulations of the bioreduction experiments it produced far superior results compared to the empirical rate formulation (equation 12.1b). Examination of equations 12.1a and 12.1b reveals that the two approaches are very similar if [Fe^{2+}] is nearly constant, which occurred in the abiotic experiments. However, in the bioreduction experiments [Fe^{2+}] ranged from 0 to tens of mg L^{-1}. The elementary rate formulation (equation 12.1a) may have performed better in the bioreduction simulations because this equation included the effect of [Fe^{2+}]. Therefore, only equation 12.1a was used to simulate the bioreduction experiments.

Fe^{2+} Sorption to S. putrefaciens *CN32*

The biosorption of 4.30 mg L^{-1} Fe^{2+} to 10^8 cells mL^{-1} of *S. putrefaciens* CN32 in PIPES-phosphate buffer at pH 6.80 ± 0.05 was experimentally shown to be an equilibrium reaction

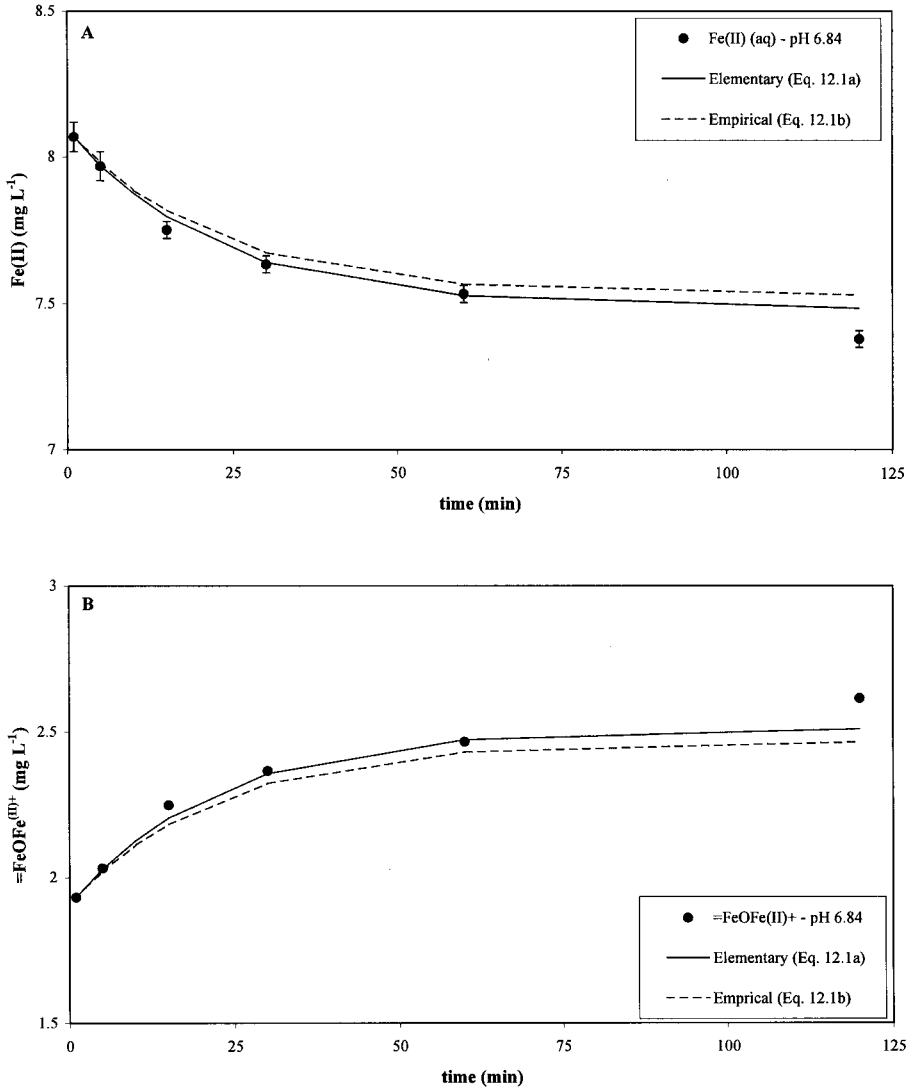

FIGURE 4 Sorption kinetics of Fe^{2+} to hematite at pH 6.84. (A) Fe(II) (aq) loss from solution over first 120 min. (B) Corresponding production $=FeOFe^{(II)+}$. Both an elementary rate formulation (equation 12.1a) and an empirical rate formulation (equation 12.1b) were used to model the experimental results. Rate parameters are given in Table 4. Error bars represent standard deviation of triplicate measurements.

(Figure 5A). The total recovery of Fe(II) was constant throughout this kinetic experiment (Figure 5A), thus system consistency was validated. The slope of the linear adsorption isotherm for Fe^{2+} biosorption to *S. putrefaciens* CN32 (Figure 5B) was 0.134 (L/10^{11} cell) ($R^2 = 0.792$). The 10^8 cells mL^{-1} *S. putrefaciens* CN32 concentration was approximated to equal $5.0(10)^{-3}$ mol L^{-1} (required units for modeling) based on an assumed molecular formula of $C_5H_7O_2N$ (=113 g mol^{-1}) and unit mass of $5(10)^{-12}$ g $cell^{-1}$. The exact value for [DIRB] was $4.4(10)^{-3}$ mol L^{-1}; however, the approximated value was used because of the assumptions involved. The value of log K_8^e was

TABLE 4 Summary of reaction rate constants for the abiotic sorption of Fe^{2+} to hematite (R_{567})

Exp. pH	Elementary rate formulation (equation 12.1a)	R^2 for Fe^{2+}(aq)	R^2 for $=FeOFe^{(II)+}$	Empirical rate formulation (equation 12.1b)	R^2 for Fe^{2+}(aq)	R^2 for $=FeOFe^{(II)+}$
6.62	$\log k^{f}_{567} = 6.94$ (M^{-1} h^{-1})	0.9149	0.9124	$k^{F}_{567} = 1.24$ M^{-1} h^{-1}	0.9070	0.9133
	$\log k^{b}_{567} = 0.47$ (h^{-1})			$k^{B}_{567} = 3.57$ h^{-1}		
6.84	$\log k^{f}_{567} = 6.37$ (M^{-1} h^{-1})	0.9785	0.9788	$k^{F}_{567} = 0.81$ M^{-1} h^{-1}	0.9775	0.9790
	$\log k^{b}_{567} = 0.19$ (h^{-1})			$k^{B}_{567} = 1.93$ h^{-1}		

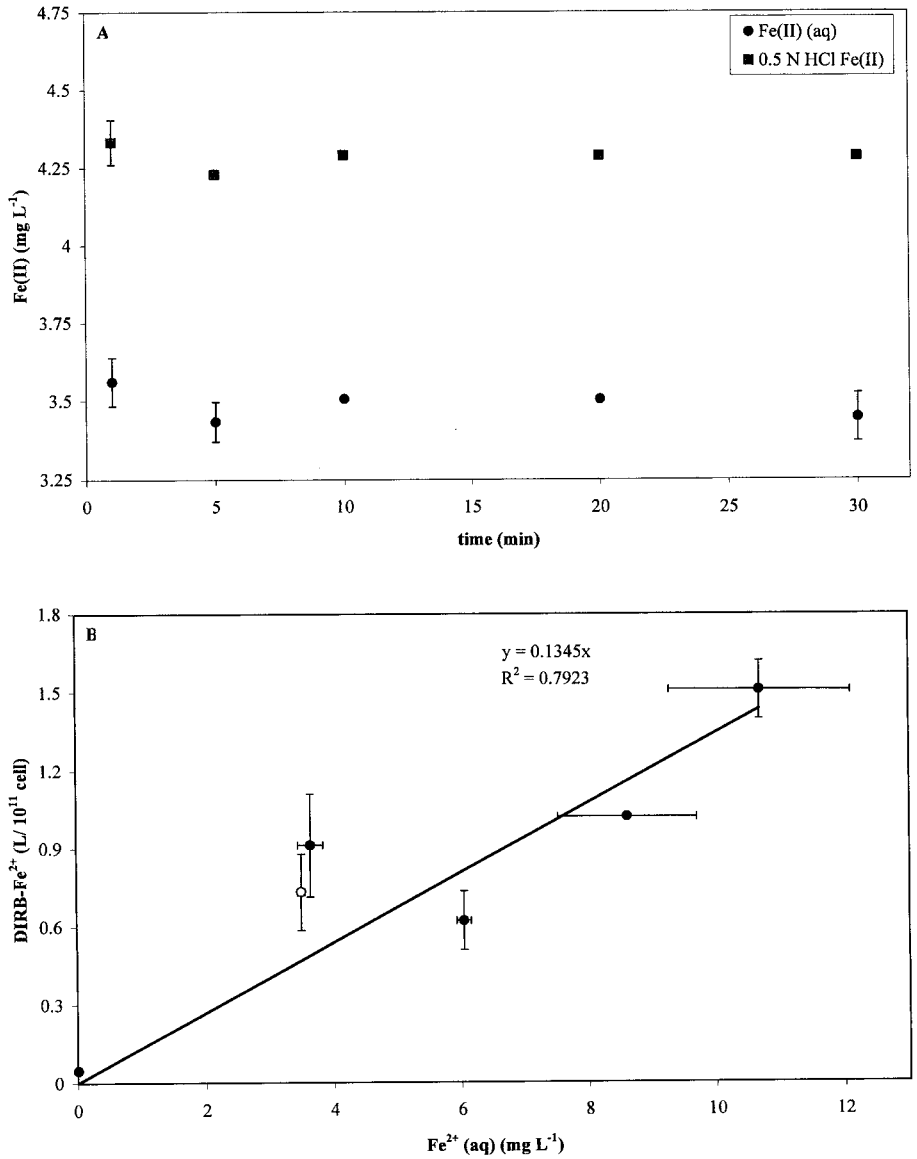

FIGURE 5 Biosorption of Fe^{2+} to *S. putrefaciens* CN32. (A) Kinetics. (B) Equilibrium isotherm. Open symbol in B is from the kinetics experiment. Error bars represent standard deviation of triplicate measurements.

calculated to equal +1.43 based on the isotherm slope and approximated value for [DIRB] (mass action equation 6.4, Table 2). The amount of Fe(II) biosorption to *S. putrefaciens* CN32 reported herein is lower by a factor of ca. 600 compared to Liu et al. (2001a). Experiments by Liu et al. (2001a) were performed at pH 7.0 in 30 mM PIPES (as compared to pH 6.8 in 50 mM PIPES) with similar cell suspension concentrations but greater Fe(II) concentrations. The growth state of the bacteria or the degree of cell flocculation may have caused some differences between these studies; however, this is speculative.

Bioreduction of Hematite by S. putrefaciens *CN32*

The kinetics of hematite bioreduction by *S. putrefaciens* CN32 under nongrowth conditions with H_2 as the electron donor was measured in four replicate experiments. The ad hoc rate constants obtained from the current experiments (i.e., linear regression of $d[Fe(II)_{TOT}]/dt$) are included in Table 1 and compare well with the literature. The formulation of reaction rates for both R1 and the lumped kinetic reactions R_{567} could have been obtained solely from these bioreduction experiments. In fact, it likely would have been easier to obtain a "better" model fit where different combinations of rate formulations for the sorption and bioreduction reactions could have been applied. However, because two of the proposed rate formulations of R_1 were based on free surface sites and R_{567} directly affected this quantity, the rate formulation for R_{567} was obtained from separate abiotic experiments (discussed previously). Also, we wanted to demonstrate that independently determined reaction-based rate formulations would be applicable in another experimental system. Thus, the predetermined rate formulation for the sorption of Fe^{2+} to hematite (equation 12.1a, Table 3) was set before attempting to formulate a rate equation for hematite bioreduction (equation 9, Table 2).

The reaction network yields mass conservation equation 8.1 (Table 2) in which all chemical species were measured so that partial system consistency was assessed for this system. Equation 8.1 is a mass balance for total Fe and while the measurement of total Fe in this experiment may seem trivial (considering the mass initially added was measured) it did satisfy the theoretical requirement to validate at least one mass conservation equation. Based on the assumed stoichiometry of R1, equation 8.2 would provide the most sensitive means of validation if both total Fe(II) produced and H_2(aq) consumed could be measured simultaneously. Several experimental challenges need to be overcome before this approach could work reliably.

Three different kinetic reaction rate formulations (equations 9.1a, 9.1b, 9.1c; Table 2) were used to simulate R1. Equation 9.1a is based on an elementary rate formulation for the overall reaction and, as shown in Figures 6 through 9, tended to better predict Fe^{2+}(aq) versus 0.5 N HCl Fe(II). This was expected because the product included in equation 9.1a is $[Fe^{2+}]$ and not total biogenic Fe(II). The elementary rate formulation also tended to further underpredict 0.5 N HCl Fe(II) as the simulation time increased (particularly after ca. 48 h). A summary of all measured data versus model predictions is presented in Figure 10 and confirms the general trend that equation 9.1a underpredicted bioreduction. Model estimates of the rate constants for all rate formulations obtained with each experiment and goodness-of-fit criterion are summarized in Table 5. These data confirm that the rate parameters obtained from each experiment were in reasonable agreement (e.g., never differed by greater than factor of three for all rate formulations).

For the elementary rate formulation, the equilibrium constants estimated from the paired forward and backward rate constants were nearly invariant $[\log(k_1^f/k_1^b) = \log K_1^e = 24.37 \pm 0.15\ (n = 4)]$. The equilibrium constant for R1 calculated from standard state thermodynamic data (Stumm and Morgan 1996) ($\Delta G^\circ = -144$ kJ mol^{-1}) was $\log K_1^e = 25.28$, which is in reasonable agreement with these model predictions.

The empirical rate formulations for R_1 (equation 9.1b based on free surface sites and equation 9.1c based on free surface sites and biosorption inhibition; Table 2) also fit the four experiments well (Figures 6–9, Table 5). Equation 9.1b tended to overpredict Fe^{2+}(aq) as the simulation time increased (e.g., Figure 6A, Figure 10); however, equation 9.1b captured long-term bioreduction kinetics better than the elementary rate formulation (equation 9.1a). This was expected because if Fe^{2+} were overpredicted then $=FeOFe^{(II)+}$ may be underpredicted and this would dampen the slowing of the reaction caused by hematite surface passivation.

TABLE 5 Summary of reaction rate constants for all replicate experiments on the biological reduction of hematite (R1)

Rep. #	Elementary rate formulation (equation 9.1a)	R^2 for Fe^{2+}(aq)	R^2 for 0.5 N HCl Fe(II)	Empirical rate formulation (equation 9.1b)—free surface sites	R^2 for Fe^{2+}(aq)	R^2 for 0.5 N HCl Fe(II)	Empirical rate formulation (equation 9.1c)—hematite surface passivation and DIRB inhibition	R^2 for Fe^{2+}(aq)	R^2 for 0.5 N HCl Fe(II)
1	$\log k_1^f = 26.30\ (M^{-4}\ h^{-1})$ $\log k_1^b = 2.00\ (M^{-1}\ h^{-1})$	0.9803	0.9766	$k_{fss} = 0.016\ h^{-1}$	0.9659	0.9570	$k_{pass} = 0.020\ h^{-1}$ $k_{inhib} = 0.030\ h^{-1}$	0.9916	0.9839
2	$\log k_1^f = 26.80\ (M^{-4}\ h^{-1})$ $\log k_1^b = 2.25\ (M^{-1}\ h^{-1})$	0.9277	0.9257	$k_{fss} = 0.030\ h^{-1}$	0.8341	0.8384	$k_{pass} = 0.040\ h^{-1}$ $k_{inhib} = 0.060\ h^{-1}$	0.9053	0.9041
3	$\log k_1^f = 26.53\ (M^{-4}\ h^{-1})$ $\log k_1^b = 2.10\ (M^{-1}\ h^{-1})$	0.9228	0.9549	$k_{fss} = 0.015\ h^{-1}$	0.9328	0.8744	$k_{pass} = 0.020\ h^{-1}$ $k_{inhib} = 0.030\ h^{-1}$	0.9666	0.9265
4	$\log k_1^f = 26.20\ (M^{-4}\ h^{-1})$ $\log k_1^b = 2.00\ (M^{-1}\ h^{-1})$	0.9746	0.9611	$k_{fss} = 0.011\ h^{-1}$	0.9489	0.9752	$k_{pass} = 0.015\ h^{-1}$ $k_{inhib} = 0.030\ h^{-1}$	0.9833	0.9944
All[a]		0.9003	0.9425		0.8895	0.8592		0.9355	0.9090

[a]Combined data analyzed from Figure 10.

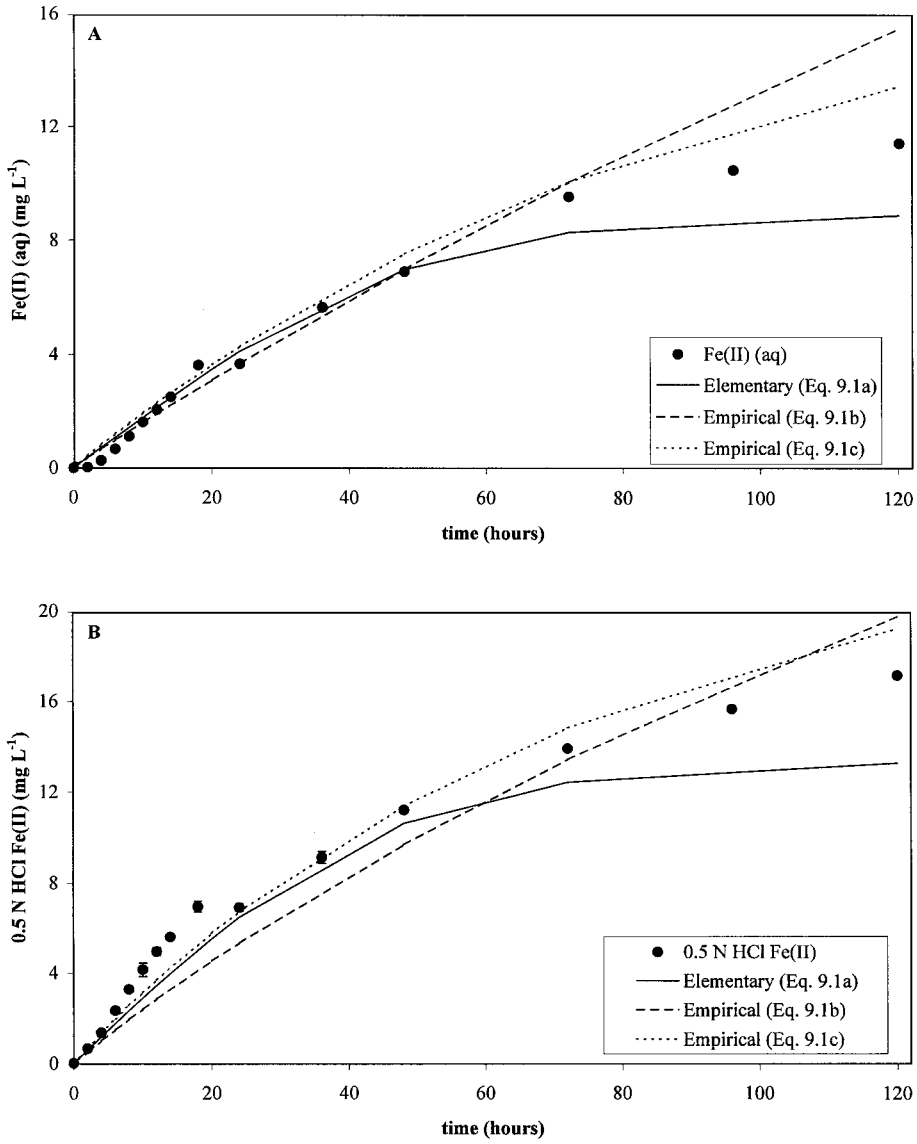

FIGURE 6 Reaction kinetics for the biological reduction of hematite—Replicate #1. (A) Production of Fe^{2+}(aq). (B) Production of 0.5 N HCl Fe(II). An elementary rate formulation (equation 9.1a) and two empirical rate formulations (equations 9.1b, 9.1c) were used to model the experimental results. Rate parameters are given in Table 5. Error bars represent standard deviation of triplicate measurements.

Based on all the measured and predicted results presented in Figure 10, no one rate formulation fit the data best but all were acceptable (R^2 values ranged from 0.83 to 0.91 for prediction of both Fe(II) (aq) and 0.5 N HCl Fe(II); Table 5). Thus, it is difficult to say which of these rate formulations (equations 9.1a–9.1c) is best. However, for the two abiotic Fe^{2+} sorption rate formulations we found that one (equation 9.1a, Table 3) performed better when combined into a more complex system. Therefore, a future test for these rate

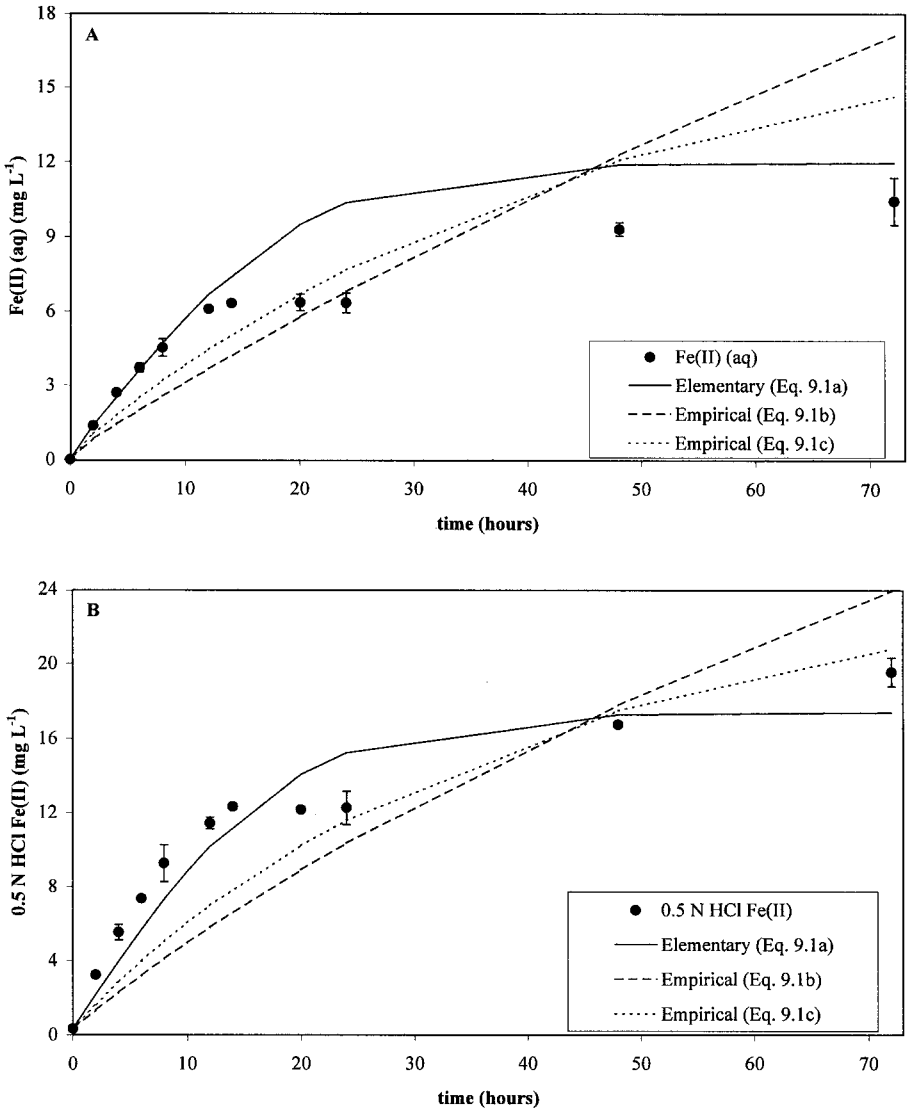

FIGURE 7 Reaction kinetics for the biological reduction of hematite—Replicate #2. (A) Production of Fe^{2+}(aq). (B) Production of 0.5 N HCl Fe(II). An elementary rate formulation (equation 9.1a) and two empirical rate formulations (equations 9.1b, 9.1c) were used to model the experimental results. Rate parameters are given in Table 5. Error bars represent standard deviation of triplicate measurements.

formulations will be to see how they perform in more complicated experiments (e.g., hematite bioreduction with AQDS in system) (Burgos et al. 2002).

Summary

The biological reduction of solid-phase ferric oxides is very complicated, making the modeling of bioreduction difficult. Considerable care was taken in designing, simplifying,

conducting, and modeling these experiments, and a reaction-based model could adequately simulate the biological reduction of hematite. The advantage of using a reaction-based model versus an ad hoc approach (Liu et al. 2001b) is that the rate formulations are theoretically descriptive of the chemical reaction and, therefore, applicable to a range of environmental conditions. Indeed, we have demonstrated that independently determined reaction-based rate formulations were applicable in another experimental

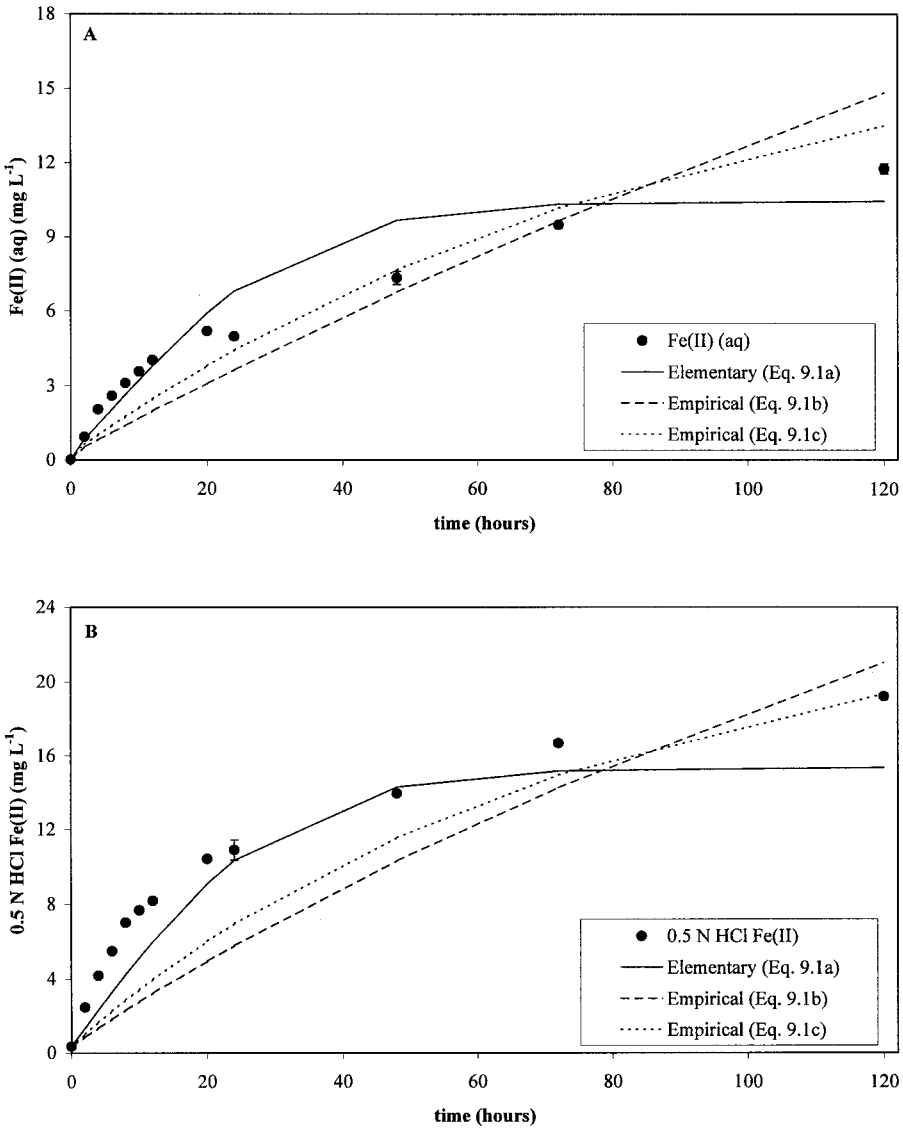

FIGURE 8 Reaction kinetics for the biological reduction of hematite—Replicate #3. (A) Production of Fe^{2+}(aq). (B) Production of 0.5 N HCl Fe(II). An elementary rate formulation (equation 9.1a) and two empirical rate formulations (equations 9.1b, 9.1c) were used to model the experimental results. Rate parameters are given in Table 5. Error bars represent standard deviation of triplicate measurements.

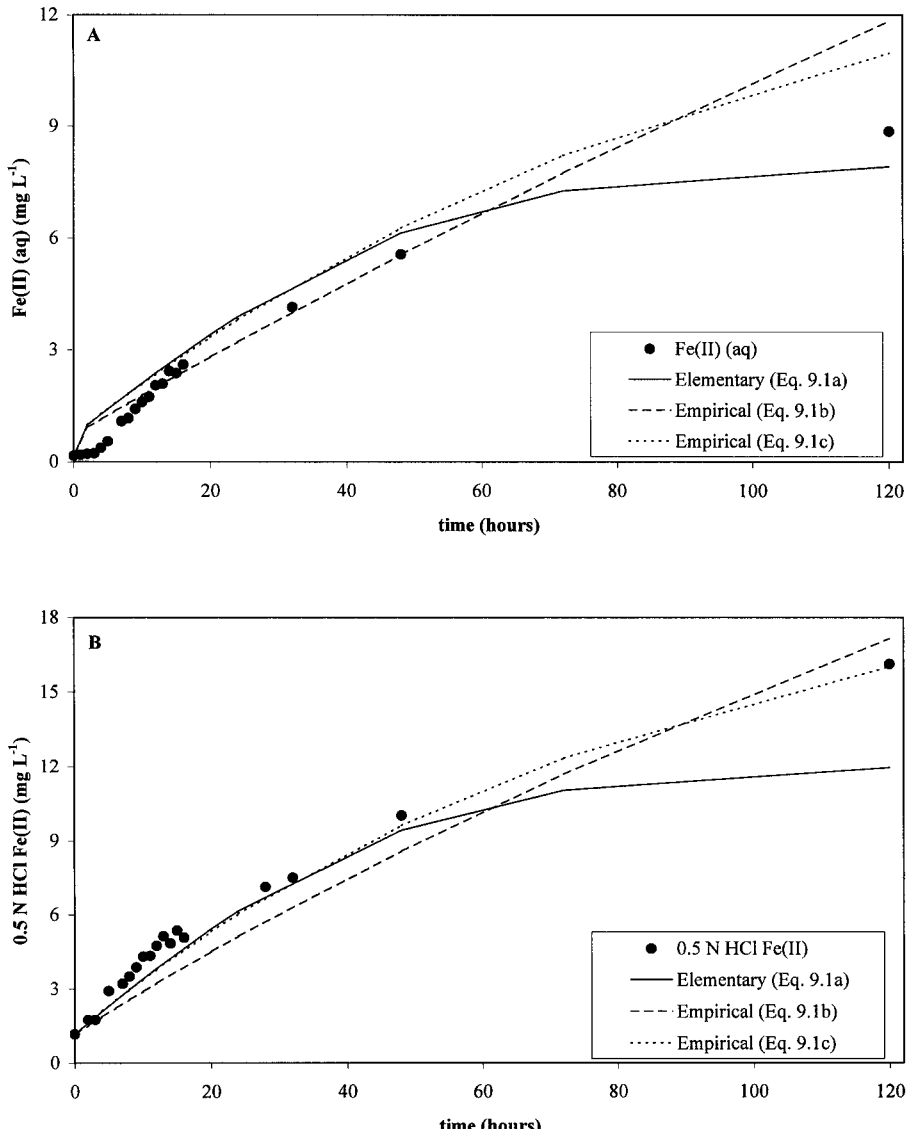

FIGURE 9 Reaction kinetics for the biological reduction of hematite—Replicate #4. (A) Production of Fe^{2+}(aq). (B) Production of 0.5 N HCl Fe(II). An elementary rate formulation (equation 9.1a) and two empirical rate formulations (equations 9.1b, 9.1c) were used to model the experimental results. Rate parameters are given in Table 5. Error bars represent standard deviation of triplicate measurements.

system. Therefore, the simulation and prediction of complex biogeochemical systems may eventually be able to be performed using reaction-based models. Complex systems will have to be decomposed into simpler subsystems. Kinetic experiments will have to be carefully designed to satisfy minimum data needs and validate partial system consistency in order to even use reaction-based models. System complexity can then be incrementally increased until ultimately field-scale flow systems can be studied.

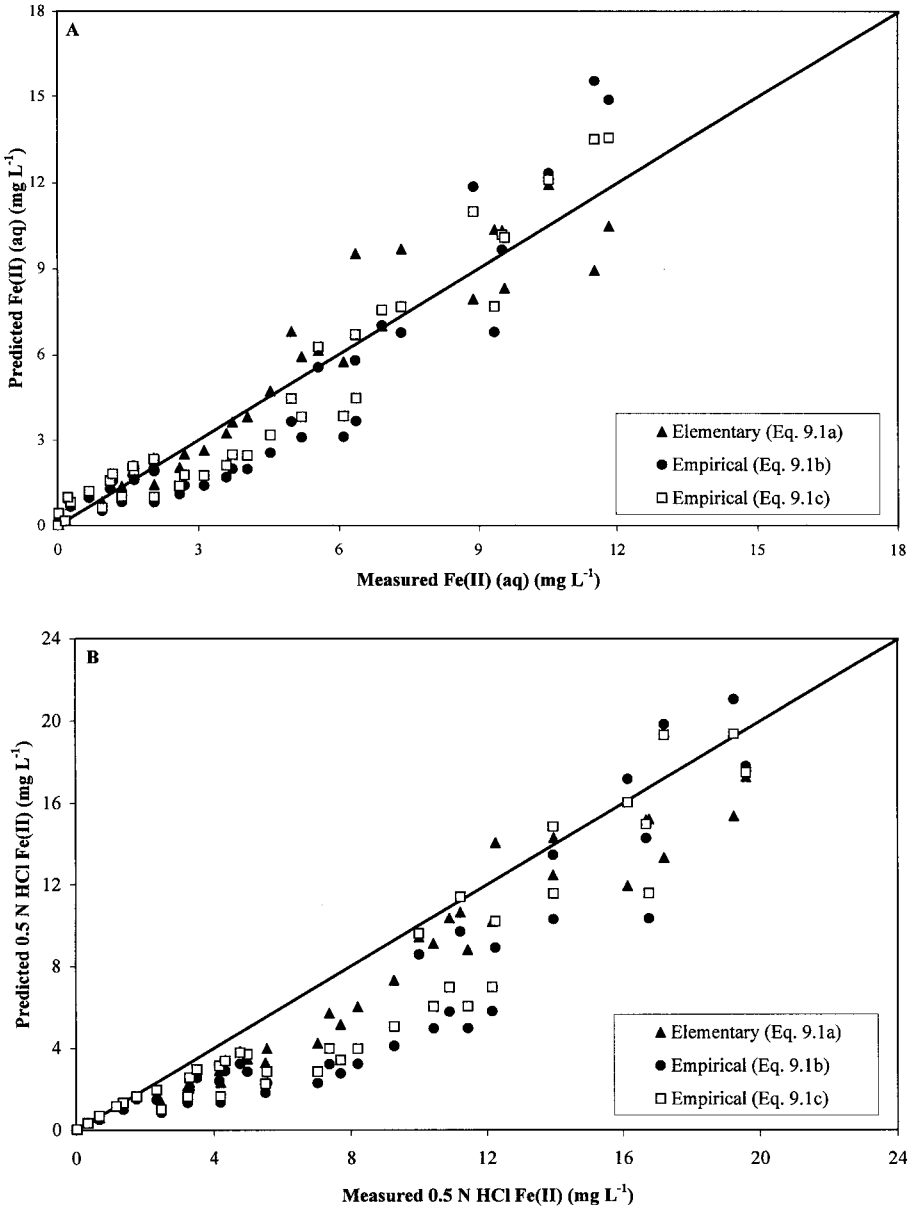

FIGURE 10 Summary of measured and predicted results for the biological reduction of hematite. (A) Prediction of Fe^{2+}(aq). (B) Prediction of 0.5 N HCl Fe(II). The diagonal line represents a 1:1 correlation. An elementary rate formulation (equation 9.1a) and two empirical rate formulations (equations 9.1b, 9.1c) were used to model the experimental results. Rate parameters are given in Table 5.

References

American Public Health Association (APHA). 1995. Standard methods for the examination of water and wastewater. Washington, DC: American Public Health Association, p 3-66–3-68, 5-7–5-8.

Arnold RG, Olson TM, Hoffman MR. 1986. Kinetics and mechanism of dissimilative Fe(III) reduction by *Pseudomonas* sp. 200, Biotechnol Bioeng 28:1657–1671.

Arnold RG, DiChristina TJ, Hoffman MR. 1988. Reductive dissolution of Fe(III) oxides by *Pseudomonas* sp. 200. Biotechnol Bioeng 32:1081–1096.

Atkins PW. 1986. Physical chemistry, 3rd ed. Oxford: Oxford University Press.

Burgos WD, Royer RA, Yeh GT, Fang YL, Fisher AS, Dempsey BA. 2002. Reaction-based modeling of quinone-mediated bacterial iron(III) reduction. Geochim Cosmochim Acta 2002, in preparation.

Caccavo F, Blakemore RP, Lovley DR. 1992. A hydrogen-oxidizing, Fe(III)-reducing microorganism from the Great Bay estuary, New Hampshire. Appl Environ Microbiol 58:3211–3216.

Chen Y. 1994. CIRF: A general coupled reaction-transport model and simulator. Ph.D. Dissertation, Department of Geological Sciences, Indiana University, Bloomington, IN. 308 p.

Chilakapati A, 1995. RAFT. A Simulator for ReActive Flow and Transport of groundwater contaminants, PNL-10636. Pacific Northwest National Laboratory, Richland, WA.

Chilakapati A, Ginn T, Szecsody JE. 1998. An analysis of complex reaction networks in groundwater modeling. Water Resources Res 34:1767–1780.

Cooper DC, Picardal F, Rivera J, Talbot C. 2000. Zinc immobilization and magnetite formation via ferric oxide reduction by *Shewanella putrefaciens* 200. Environ Sci Technol 34:100–106.

Coughlin BR, Stone AT. 1995. Nonreversible adsorption of divalent metal ions (Mn^{II}, Co^{II}, Ni^{II}, Cu^{II}, an Pb^{II}) onto Goethite: Effects of acidification, Fe^{II} addition, and picolinic acid addition. Environ Sci Technol 29:2445–2455.

Curtis GP, Reinhard M. 1994. Reductive dehalogenation of hexachloroethane, carbon tetrachloride, and bromoform by anthrhydroquinone and humic acid. Environ Sci Technol 28:2393–2401.

Dzombak DA, Morel FMM. 1990. Surface complexation modeling: hydrous ferric oxide. New York: Wiley. 15 p.

Fang Y, Yeh GT, Burgos WD. 2002. A numerical model of reaction-based biogeochemical processes—model description and example simulations. Water Resources Res Submitted.

Fredrickson JK, Zachara JM, Kennedy DW, Dong H, Onstott TC, Hinman NW, Li SW. 1998. Biogenic iron mineralization accompanying the dissimilatory reduction of hydrous ferric oxide by a groundwater bacterium. Geochim Cosmochim Acta 62:3239–3257.

Fredrickson JK, Zachara JM, Kennedy DW, Duff MC, Gorby YA, Li SW, Krupka KM. 2000. Reduction of U(VI) in goethite (α-FeOOH) suspensions by a dissimilatory metal-reducing bacterium. Geochim Cosmochim Acta 64:3085–3098.

Heijman GC, Grieder E, Holliger C, Schwarzenbach RP. 1995. Reduction of nitroaromatic compounds coupled to microbial iron reduction in laboratory aquifer columns. Environ Sci Technol 29:775–783.

Jeon B-H, Dempsey BA, Burgos WD, Royer RA. (2001). Reactions of ferrous iron with hematite. Colloid and Surfaces A 191:41–55.

Kim S, Picardal FW. 1999. Enhanced anaerobic biotransformation of carbon tetrachloride in the presence of reduced iron oxides. Environ Toxicol Chem 18:2142–2150.

Klausen J, Trober SP, Haderlein SB, Schwarzenbach RP. 1995. Reduction of substituted nitrobenzenes by Fe(II) in aqueous mineral suspensions. Environ Sci Technol 29:2396–2404.

Knapp RB. 1989. Spatial and temporal scales of local equilibrium in dynamic fluid-rock systems. Geochim Cosmochim Acta 53:1955–1964.

Lasaga AC. 1998. Kinetic theory in the earth sciences. Princeton, NJ: Princeton University Press. 728 p.

Liu C, Zachara JM, Gorby YA, Szecsody JE, Brown CF. 2001a. Microbial reduction of Fe(III) and sorption/precipitation on *Shewanella putrefaciens* strain CN32. Environ Sci Technol 35:1385–1393.

Liu C, Kota S, Zachara JM, Fredrickson JK, Brinkman CK. 2001b. Kinetic analysis of the bacterial reduction of goethite. Environ Sci Technol 35:2482–2490.

Lovley DR. 1993. Dissimilatory metal reduction. Ann Rev Microbiol 47:263–290.

Lovley DR, Goodwin S. 1988. Hydrogen concentrations as an indicator of the predominant terminal electron-accepting reaction in aquatic sediments. Geochim Cosmochim Acta 52:2993–3003.

Lovley DR, Phillips EJP. 1988. Novel mode of microbial energy metabolism: organic carbon oxidation coupled to dissimilatory reduction of Fe or manganese. Appl Environ Microbiol 54:1472–1480.

Lovley DR, Fraga JL, Blunt-Harris EL, Hayes LA, Phillips EJP, Coates JD. 1998. Humic substances as a mediator for microbially catalyzed metal redcution. Acta Hydrochim Hydrobiol 26:152–157.

Lovley DR, Woodward JC, Chapelle FH. 1994. Stimulated anoxic biodegradation of aromatic hydrocarbons using Fe(III) ligands. Nature 370:128–131.

Nevin KP, Lovley DR. 2000. Lack of production of electron-shuttling compounds or solubilization of Fe(III) during reduction of insoluble Fe(III) oxide *Geobacter metallireducens*. Appl Environ Microbiol 66:2248–2251.

Roden EE, Lovley DR. 1993. Dissimiliatory Fe(III) reduction by the marine microorganism Desulfuromonas acetoxidans. Appl Environ Microbiol 59:734–742.

Roden EE, Zachara JM. 1996. Microbial reduction of crystalline Fe^{3+} oxides: Influence of oxide surface area and potential for cell growth. Environ Sci Technol 30:1618–1628.

Roden EE, Urrutia MM. 1999. Ferrous iron removal promotes microbial reduction of crystalline iron(III) oxides. Environ Sci Technol 33:1847–1853.

Salvage KM, Yeh GT. 1998. Development and application of a numerical model of kinetic and equilibrium microbiological and geochemical reactions (BIOKEMOD). J Hydrol 20:927–952.

Steefel CI, MacQuarrie KTB. 1996. Approaches to modeling of reactive transport in porous media, Reviews in mineralogy, vol. 34. Reactive transport in porous media (Lichtner PC, Steefel CI, Oelkers H), Washington, DC: Mineralogical Society of America, p 84–129.

Steefel CI, van Cappellen P. 1998. Preface: reactive transport modeling of natural systems. J Hydrol 209:1–7.

Stumm W, Morgan JJ. 1996. Aquatic chemistry, 3rd ed. New York: Wiley. 535 p.

Tamura H, Goto K, Yotsuyanagi T, Nagayama M. 1974. Spectrometric determination of iron(II) with 1,10-phenanthroline in the presence of large amounts of iron(III). Talanta 21:314–318.

Trivedi P, Axe L. 2000. Modeling Cd and Zn sorption to hydrous metal oxides. Environ Sci Technol 34:2215–2223.

Urrutia MM, Roden EE, Fredrickson JK, Zachara JM. 1998. Microbial and surface chemistry controls on reduction of synthetic Fe(III) oxide minerals by the dissimilatory iron-reducing bacterium *Shewanella alga*. Geomicrobiol J 15:269–291.

Urrutia MM, Roden EE, Zachara JM. 1999. Influence of aqueous and solid-phase complexants on microbial reduction of crystalline iron(III) oxides. Environ Sci Technol 33:4022–4028.

Wildung RE, Gorby YA, Krupka KM, Hess NJ, Li SM, Plymale AE, McKinley JP, Fredrickson JK. 2000. Effect of electron donor and solution chemistry on products of dissimilatory reduction of technetium by *Shewanella putrefaciens*. Appl Environ Microbiol 66:2451–2460.

Yeh GT, Tripathi VS. 1989. A critical evaluation of recent developments in hydrogeochemical transport models of reactive multichemical components. Water Resources Res 25:93–108.

Yeh GT, Burgos WD, Zachara JM. 2001. Modeling and measuring biogeochemical reactions: system consistency, data needs, and rate formulations. Adv Environ Res 5:219–237.

Zachara JM, Fredrickson JK, Li SM, Kennedy DW, Smith SC, Gassman PL. 1998. Bacterial reduction of crystalline Fe^{3+} oxides in single phase suspensions and subsurface materials. Amer Mineral 83:1426–1443.

Zachara JM, Smith SC, Fredrickson JK. 2000. The effect of biogenic Fe(II) on the stability of $Co(II)EDTA^{2-}$ to goethite and a subsurface sediment. Geochim Cosmochim Acta 64:1345–1362.